Testing Structure-from-Motion imaging technique to quantify Blue mussels (*Mytilus spp.)* abundance

Thord Håkon Bakke

Master thesis in Aquaculture

Department of Biological Sciences (BIO)

University of Bergen

June 2023

2023

Testing Structure-from-Motion imaging technique to quantify Blue mussels (Mytilus spp.) abundance

University of Bergen

Acknowledgements

I would like to express my gratitude to my supervisors at the Institute of Marine research, Antonio Garcia and Tore Strohmeier, for their continuous guidance, invaluable feedback, and relentless encouragement throughout this work. Their expertise and commitment have been crucial in shaping my master's journey. I also want to acknowledge and thank Thorolf Magnesen, my internal supervisor at the University of Bergen, for his valuable guidance during my research.

I also want to thank my family and partner, who have provided steady support and love throughout this challenging journey. Their constant belief in my abilities and tireless encouragement have been a source of strength and inspiration.

Lastly, I want to extend my sincerest thanks to my classmates, in particular, the lads at my study hall for who has been a pillar of support during this journey. Their presence, understanding, and constant encouragement have been invaluable to me, providing much-needed comfort during the most challenging times of this journey.

Thank you all for your solid faith in my abilities and for your constant comfort that has made this accomplishment possible. This thesis would not have been achievable without your continuous support and belief in me.

Abstract

Recent reports have highlighted changes in the population dynamics of blue mussels, emphasizing the necessity of gathering quantitative data on a large scale. This would help determine whether the population of intertidal mussels is exhibiting changes over time, surpassing the natural variability inherent in these ecosystems. This work aims to establish a systematic procedure for obtaining quantitative data on blue mussel dynamics leveraging information from 3D models generated through the Structure-from-Motion. The study sought to correlate fieldwork-collected datasets (biomass and length distribution) and complexity metrics (vector dispersion, fractal dimension and rugosity) derived from these 3D models. A weak linear relationship between complexity metrics and biological metrics was observed, although both groups showed substantial internal correlation. Principal component analysis of each group did not reveal clear grouping, indicating limited variability among the metrics. The principal component regression analysis revealed that a significant proportion of the variation, particularly in biomass, could be explained by the first five principal components derived from the complexity metrics.

The canonical correlation analysis further confirmed the potential relationship between complexity metrics and biological metrics. Notably, the fractal dimension metric appeared to be the most impactful complexity metric. Employing this metric at an ultra-high resolution could have the potential to accurately capture microscale details, although it might require an increased computational power. However, to gain a more extensive and thorough comprehension of surface complexity, it is recommended that this metric be employed alongside other complexity measurements. Despite several challenges, including small sample sizes, homogeneity of mussels, and photo quality, the results demonstrate the potential of Structure-from-Motion as a method for generating 3D models. Future research should focus on enhancing the consistency of image capture, employing calibrated cameras to boost accuracy, and conducting in-depth analyses to identify the complexity metrics that most effectively quantify microscale surface complexity. Moreover, once a reliable workflow is established, integrating machine learning algorithms for object detection could enhance its efficiency. This enhancement, when combined with the application of the SfM technique and the extensive surveying capabilities of drones, could present a powerful method for gathering comprehensive quantitative data on the dynamics of blue mussels.

List of Abbreviations

IMR	Institute of Marine Research
SfM	Structure-from-Motion
BM	Biological metrics
CM	Complexity metrics
FD	Fractal dimension
VD	Vector dispersion
PCA	Principal component analysis
PCs	Principal components
PCR	Principal component regression
CCA	Canonical correlation analysis
ROVs	Remotely Operated Vehicles
UAVs	Unmanned Aerial Vehicles
RMSEP	Root Mean Square Error of Prediction

Table of Contents

1 Introduction

1.1 Background for the project

Based on a general concern for the disappearances and population changes of a key intertidal species (Andersen et al., 2016), the Institute of Marine Research (IMR) established a monitoring program for blue mussel populations along the Norwegian coast in 2020. The objective of the program is to elucidate if the abundance of intertidal mussels is changing over time beyond the inherent randomness and natural variation in the ecosystems. In the programs first year a method for monitoring blue mussels was developed (Strohmeier et al., 2022), and the potential for new technology (i.e. images and machine learning) to monitor the populations was reviewed. Acquiring quantitative data trough efficient methods is necessary to gain a better understanding of the population dynamics of blue mussels. The presence of blue mussels has been confirmed extensively along the Norwegian coast, from secluded fjords to the more exposed coastal areas (Strohmeier et al., 2022). The widespread distribution of blue mussels along the Norwegian coast can be attributed to a variety of factors, including the species' reproductive strategy, ocean currents, and the availability of suitable habitats (Demmer et al., 2022). In light of the persistent environmental transformations driven by climate change and human activities (Berge et al., 2005), combined with the broad dispersion of mussels across coastal regions, it is becoming increasingly crucial to collect quantitative information over large areas to efficiently track these alterations.

Traditional methods to acquire quantitative data about blue mussels distribution and abundance has been time-consuming and there are novel methods that possibly can gain the same or a broader insight more efficiently. Using both flying drones and underwater ROVs (Remotely Operated Vehicle) are becoming more and more common when collecting data within a broad range of industries, and they are increasingly used to map marine resources and habitats (Ventura et al., 2023). Today, there are a broad range of affordable low-altitude airborne sensors available, with the capacity to collect imagery and bathymetric information which are comparable to information collected from more expensive LiDAR techniques which uses light in the form of a pulsed laser to measure distances (Casella et al., 2017). Using methods such as Structure-from-Motion (SfM) based on captured images might be an effective method to

gain this data. Developing this method is therefore one of the targets of the project. Combining this approach with the capacity of machine learning algorithms to detect objects could present a potent tool for enhancing the monitoring of blue mussels.

1.2 What are blue mussels?

Blue mussel (*Mytilus spp.*) is a medium size marine bivalve mollusc in the family of Mytilidae, more commonly referred as mussels. The mussel has two shell valves that are similar in size and triangular in shape. These valves are attached together at the anterior by the means of ligament and this area is called umbo. The adult mussels are sessile. Blue mussels have separate sexes and releases eggs and sperm into the water column for fertilization. Individual females can produce between 7 to 40 million eggs, depending on shell length. However, one study suggests that only 1 % of larvae reach adulthood (Thompson, 1979). Typically, spawning occurs biannually in spring and autumn. The exact timing of spawning is contingent on food availability, hence its correlation with phytoplankton blooms (Beyer et al., 2017).

Mussels are a type of meroplankton, which implies that they undergo both pelagic and benthic phases during their life cycle. The life cycle of mussels consists of two planktonic stages and two settling stages. The initial settling stage occurs when the planktonic mussel larvae develop their foot, which enables them to crawl over surfaces and adhere to them using byssus threads. They would typically attach themselves to larger algae to access space and food, as there is studies that suggests that there may be less competition for resources in among seaweed than within mussel banks with larger mussels (Newell & Moran, 1989). Once the juvenile mussels have grown to about 1-1.5 mm in size, they return to the planktonic stage and settle a second time. During this stage, they would typically adhere to a more stable substrate such as rocks, piers or other shells, forming clusters or banks (Newell & Moran, 1989). Blue mussels have the potential to live for almost 20 years and can reach lengths of up to 10 cm. However, it is rare for mussels to exceed 8 cm in length or live beyond 10 years (Beyer et al., 2017).

Blue mussels are found in temperate waters all over the world and are subject for both harvesting and intensive aquaculture (Goldberg, 1975). In Norway, they are found throughout the whole coast. They often form mussel beds (Figure 1.1) in sub littoral and littoral zones.

These mussels beds can become several centimetres thick (Baxter et al., 2022). Blue mussels tolerate a large variation in both temperature and salinity. They are suspension feeders and feed on phytoplankton and other inorganic and organic particles by pumping and filtering large volumes of water over their large ciliated gills. This seawater filtration makes the species suitable as a bioindicator in coastal waters since they also efficiently accumulate pollutants from seawater (Goldberg, 1975).

Figure 1.1: Large mussels beds during low tide in the Hardanger Fjord, Norway.

1.3 Why are blue mussels important?

1.3.1 Blue Mussels role in the ecosystem

A definition of an ecosystem is any unit that includes all organisms that function together in a given area interacting with the physical environment so that the flow of energy leads to clearly defined biotic structure and cycling of materials between living an non-living parts (Lin & Lin, 2006). Changes within an ecosystem can be a result of naturally occurring events. However, pollution or environmental change due to human activity often imposes stress to these systems (Loeb & Spacie, 1994). In an aquatic ecosystem, different organisms provide varied degree of ecological services. Blue mussels are considered as one of the more ecologically important species as they provide a broad set of essential ecological services that can also alter the effect of human activity on aquatic ecosystems (Beyer et al., 2017). They are often referred to as "ecosystems engineers" because of the way they modify their habitat, making it more suitable for themselves but also other organisms. They increase biodiversity in a habitat by providing a substrate for algae and refuge for small animals. Given the fact that they are suspension feeders and therefore consume particulate matter from the water column they clear, this species clear the water by removing phytoplankton, bacteria and fungi attached to non-living organic particles (Smaal et al., 2019). Furthermore, by filtering phytoplankton, including toxic algae, blue mussels can inhibit or prevent harmful blooms (Mafra et al., 2010). The shells they leave behind also work as an important habitat for other species, sheltering them from predation, trapping sediment, and creating refuge. The mussels are also an important source of food for a broad range of species (Norling, 2009).

Being an important habitat builder for many species of algae and fauna, beds of blue mussels sustain a high biodiversity and are therefore resilient to disturbances. Blue mussels also play a role in carbon storage (Filgueira et al., 2019; Sea et al., 2022), and this is assumed to be related to carbon stored in the mussel beds. Blue mussels role in the CO_2 cycle has been assessed as the balance between respiration, shell calcium carbonate sequestration and CO_2 release during biogenic calcification. However, this assessment ignores the ecosystem interactions that occur at population level, which can significantly alter the CO_2 cycle. Furthermore, their potential role differs in the context of non-harvested vs. harvested population, given the fact that harvesting represents a net extraction of mussels from the ocean (Filgueira et al., 2019).

However, the amount of carbon from decomposed mussels that is actually sequestrated for the future has been considered to be minimal (Gundersen et al., 2017).

Additionally, mussels can mitigate the ongoing eutrophication of the oceans caused by human activities due to its filter-feeding capabilities. Eutrophication is considered a serious threat to aquatic ecosystems all over the world (Chislock et al., 2013). In the Baltic sea as much as 97 % of the open sea is considered affected by eutrophication (HELCOM, 2018). Eutrophication is particularly prominent in semi-closed estuaries and regional seas. Excessive amounts of phosphorus and nitrogen from both present sources and pollution from the past leads to massive algae blooms (Kotta et al., 2020). The result of this is a widespread increase of hypoxia and anoxia and an increasing vulnerability to ocean acidification which again leads to loss of biodiversity and ecosystem functions and services (Malone & Newton, 2020). The impact of a raising global mean sea temperature also enhances this effect and can lead to expanded dead zones and increased risk for cyanobacteria blooms (Meier et al., 2017). Blue mussels can reduce the effect of eutrophication by being harvested and used for food, fertilizer and animal feed. The excessive nutrients that have been accumulated within the mussels will then be removed from the system and mitigate the eutrophication process (Kotta et al., 2020).

Another vital service of blue mussels, is the ability they have to take up, and thereby remove, organic pollutants and toxic substances from the water (Beyer et al., 2017). They were among the first species used to assess the environmental quality of seawater (Anonymous, 1886). Given its filter feeding habits, the mussels can reduce the amount of cyanobacteria, phytoplankton and toxins in the water column. Thus, contribute to filtering, water purification and removing of hazardous substances. Mussels have the capacity to store quite large amounts of toxins without being affected themselves (Gundersen et al., 2017). Due to their abilities, mussels are widely used as bioindicators of environmental health and quality of an ecosystem. Bioindicators are defined as organisms that respond to change in the coastal system, including pollutants and environmental stressors, and can therefore provide valuable information (Poulsen et al., 2021).

In the brackish Baltic sea, blue mussels live under low-salinity conditions. However, they are still very abundant (Westerbom et al., 2002). The blue mussels constitute of 70 % of the coastal biomass in the Baltic, which therefore contribute greatly to the ecosystems structure and function (Gundersen et al., 2017). For decades, policy initiatives to reduce external nutrient

loads have so far failed to control eutrophication of the Baltic sea, which is caused by a release of significant amounts of phosphorus and nitrogen. To mitigate this problem, protecting the blue mussels is considered an important measure. Another promising measure is farming and harvesting of the native species to further mitigate eutrophication in the Baltic sea. Harvesting farmed mussels can be a cost-effective complement to land-based measures by increasing the nutrient removal in the Baltic sea (Kotta et al., 2020).

1.3.2 Cultural and economic value of blue mussels

In 2022, global bivalve mollusc exports were valued at USD 4.3 billion, with mussels, specifically those from the Mytilidae family, contributing to 6.2% of total live weight mollusc production (FAO, 2022). They are found in the intertidal zones worldwide, and their presence is deeply rooted in the culinary and cultural heritage of numerous coastal communities. Archaeological evidence suggests that human consumption of blue mussels dates back to the Mesolithic era, around 10,000–5,000 BCE (Andersen, 2014). This species has been particularly prevalent in European cuisines and maintains cultural relevance among many indigenous tribes in North America (Deur & Turner, 2006). Historically, blue mussels have been used more frequently as bait than for direct human consumption. Nonetheless, their nutritional value is considerable, being rich sources of Vitamin B-12, selenium, manganese, and containing a healthy proportion of Omega-3 fatty acids (Gundersen et al., 2017). The recreational activity of blue mussel picking, a cultural service intrinsic to many coastal societies, offers individuals the satisfaction of gathering their own food. Mussel beds also enhance the aesthetic appeal for divers and snorkelers and contribute to maintaining water quality suitable for swimming (Gundersen et al., 2017).

The majority of mussels gathered prior to the 19th century came from wild mussel beds (Lovshin, 1996). However, the requirement for storing and distributing fishing products led to the beginning of mussel aquaculture in the 19th century. Since then, this sector of the economy has experienced significant growth, with aquaculture producing 1.11 million tonnes of live weight mussels (Mytildae) in 2020. The most common practices of mussels farming include longline culture, raft culture and bottom culture (FAO, 2022). Historically, there has not been much blue mussel cultivation in Norway. Nevertheless, 2163 tons were produced in 2021 (Fiskeridirektoratet, 2021), and the sector has started looking into the possibility of using mussels as fish feed. This might result in an increased demand for mussels, which could be

profitable for mussel farms (Torrissen et al., 2018). In recent years, there has been increased interest in integrating blue mussel aquaculture with other form of marine farming, such as seaweed cultivation and fish farming. This approach is called Integrated Multitrophic Aquaculture (IMTA) and aims to create a more sustainable and efficient system by using the waste products of one species to benefit the others (Reid et al., 2020).

1.4 Status on population today

There has been an increasing concern about the decrease in blue mussels population in the Nordic countries, in particular in the coastal waters of Eastern Norway and Western Sweden (Baden et al., 2021). This is based on reports from both scientists and people collecting mussels themselves. On the Swedish coast, the wild stocks of blue mussels have disappeared despite any reports about overharvesting in the area. Based on observations, disappearances began already in the late 1990s, but with the biggest drop in the 2000s (Baden et al., 2021). There have also been reports about disappearing and mortality of adult blue mussels from the Norwegian coast (Mortensen et al., 2021; Strohmeier, Tore et al., 2022).

However, it is not only in Norway that there has been reports that the blue mussel population might be changing. There has been reports that the distribution of the blue mussel population in the North Atlantic is changing. In the west North Atlantic, blue mussels have now been observed as far north as Svalbard, after a 1000 year absence. This was made possible due to the unusual high northward mass transport of warm Atlantic water resulting in higher sea-surface temperatures along the coast of Svalbard (Berge et al., 2005). On the other side of the Atlantic, the distribution range of the blue mussel is also changing. Along the southern portion of its range, blue mussel populations have experienced very high mortality that has been directly associated with high summer temperatures. The southern range edge of blue mussel has undergone a geographic contraction over the last five decades, resulting in a shift of approximately 350 km to the north of its previous limit at Cape Hatteras in North Carolina (Jones et al., 2010). Blue mussel populations in the Gulf of Maine have also been shown to be significantly declining over the past few decades. Numerous factors, including an increased predation by invading species, habitat modification, and climate change, have been connected to this reduction (Ruiz et al., 2011). The decrease of blue mussel populations have been linked to climate change, diseases, habitat disruption and predation (Baden et al., 2021). However,

the reason for the possible reduction in Norway has yet not been identified. It has been suggested that hybridisation with other Mytilus species could be the cause, but at the southeast coast of Norway *M. edulis* is the only species present. This disputes the fact that a hybridization might be the cause (Brooks & Farmen, 2013).

Traditionally, blue mussels have not been extensively monitored in Norway and there is limited knowledge about the natural variation of the species. However, one study analysed changes in the occurrence of mussels in the outer Oslofjord based on data from the programs "Økokyst" and "Lange tidsserier". This analysis showed a decrease in the occurrence of adult shells for the period 1990-2013. In contrast to adult mussels, juvenile mussels showed a steady increase in occurrences for the period 1990-2020 (Nøland, 2021). In general, previous investigation form a limited starting point for comparing data on development of the stock.

Investigations carried out in 2021 and 2022 shows that blue mussels occur in every region, from deep within the fjord to the exposed coastline of Norway. The Oslofjord has the least continuous occurrences of mussels, and in the middle and inner part of the fjord there is a dominance of older mussels indicating that there has been a limited recruitment into the stock. Preliminary results show that blue mussel distribution is not directly determined by environmental factors alone. Within all regions, there are many different microhabitats within the intertidal zone, with also the occurrence of predators changing throughout the coast. All of these factors must be taken into consideration over time to determine changes in the stock and the reason for the changes (Strohmeier et al., 2022).

Nonetheless, merely documenting the presence of blue mussels may not provide a comprehensive understanding of the shifts in their population dynamics. Integrating quantitative data about biological metrics(BM), such as biomass, size, and numbers, helps describe the population's dynamics while also connecting these parameters to the significant ecosystem services that blue mussels provide. For example, the population's biomass delivers insights into the total organic matter the mussels produce, explaining their ecological productivity and filtration capacity (Riisgård et al., 2014). Moreover, the length distribution in the population provides critical information regarding the age structure, growth rates, and mortality patterns, which is instrumental in projecting future population trends (Seed, 1992). Gathering data on the abundance of blue mussels represents another critical aspect of their population dynamics. This provides vital insights into their reproductive success, mortality

rates, and spatial distribution. For example, high population numbers may suggest conditions favourable to reproduction, low predation, and decreased mortality from disease or environmental factors, collectively demonstrating a robust and stable population (Suchanek, 1992).

1.5 Structure-from-motion

High-resolution topography has normally been associated with high costs and logistics, but with the rapid on-going technological revolution, more affordable options have emerged (Westoby et al., 2012). Traditionally, 3D photogrammetry based on 2D photos relied on stereoscopic photos, which means that a scene had to include specified targets with known 3D positions (Snavely et al., 2007). There are also more modern methods such as the use of LIDAR, but this is quite time-consuming and requires specialized personnel and equipment (Jaboyedoff et al., 2012). SfM, on the other hand, is a low-cost and user-friendly photogrammetric technique that generates high-resolution 3D models by a bundle adjustment procedure based on identification of matching features in multiple overlapping, offset images. The recent advance in computers processing capacity has made that processes, that previously required very expensive computers, now can be done on personal computers with standard specifications (Leiserson et al., 2020).

There are several application software's such as Meshroom (AliceVision, 2018) and Agisoft Metashape (Agisoft, 2022) that are able to create 3D mesh models from a set of 2D photographs. Some of the application software also support cloud computing, which is very beneficial when operating with large data sets, and much of the mesh creation can be done on remote servers. Meshroom is a free, open-source 3D reconstruction software based on the AliceVision framework. It is available for both Windows and Linux. The program has been designed to easily obtain a 3D model from multiple images with minimal user interaction, and to also provide advanced users a solution where it is possible to modify to suit their creative or technical needs (Griwodz et al., 2021). In other words, you do not need any previous experience to use this program. The resulting 3D model generated by SfM can be exported and further analysed in other programs such as Rhinoceros 3D to calculate the complexity metrics (CM) giving information about the 3D model. Rhinoceros 3D is a commercial 3D computer graphics

and computer-aided design software that was developed by Robert McNeel and Associates (McNeel, 2010).

1.6 Drones/Cameras

The use of drones, or unmanned aerial vehicles (UAVs), for collecting quantitative data has become increasingly popular in recent years due to numerous advantages over traditional data collection methods (Portosi et al., 2019). One of the key advantages of using drones for data collection is their ability to cover large areas in a short amount of time (Sousa & Gonçalves, 2011). Normally, to collect images of blue mussels, there has been a need to manually go to each mussel patch to acquire the photos for data collection. Using drones will make this operation more efficient and smooth.

Another advantage of using drones for data collection is their ability to access areas that are difficult or even impossible to reach by any other means. For example, if the terrain is rugged and challenging for humans to access, drones can be a good option to collect data in these areas. Due to UAVs increased popularity, their price has significantly decreased in recent years, making it more accessible to a wider range of users. This has led to an increased accessibility to applications for drones, such as aerial photography and videography (van der Merwe et al., 2020). On the other side, drones can easily be affected by the weather and if it is strong wind or rain, the use of drones can be difficult. Additionally, when using drones you do not have the possibility to do anything hands on, such as removing algae covering the mussels, and one is limited to the visible tidal sone. With flying drones the time of operation can be a limiting factor, but this is steadily increasing with advancements in battery technology.

1.7 Machine learning and object detection

Machine learning is known as a subfield of artificial intelligence that enables computers to learn and improve without being explicitly programmed. One of the most significant applications used in a broad set of fields is object identification, which involves training algorithms to recognize objects in images or videos. Object identification includes several steps, such as data collection, data pre-processing, model training and model testing (Reig et al., 2020).

As a part of the IMR project, an evaluation of machine learning programs for identifying blue mussels was conducted. After reviewing several annotation programs, VIAME was selected for its advantageous capabilities. Annotation for machine learning from photos can be categorized into three types: classification, object detection, and segmentation, each providing different time of annotation for training the algorithm to recognize mussels. U-Net was utilized as the program for training the algorithm, and initial results indicate that the algorithm can recognize mussels patches. However, further annotation work is necessary to enhance the algorithms accuracy. The incorporation of this automation into the workflow has the potential to enhance the efficiency of the image analysis process. Integrating machine learning will eliminate the manual selection of mussels and provide masked photos with mussels. This optimized workflow, which visually represents this integration, can be viewed in Figure 1.2.

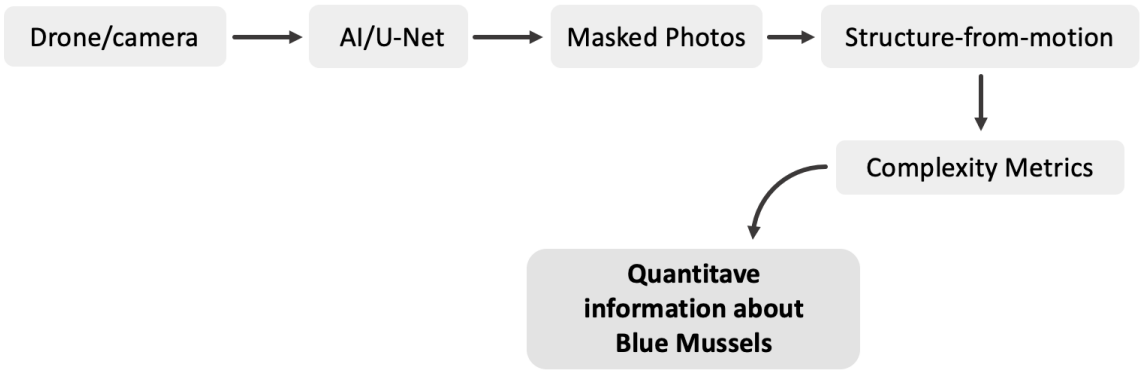

Figure 1.2: The workflow implemented with artificial intelligence (machine learning), trained by U-net to automate and improve the performance of the method.

1.8 Aim of study (Objectives)

The primary aim of this study, conducted in collaboration with the Institute of Marine Research, was to explore and test emerging technologies, specifically drones/cameras and Structure-from-Motion (SfM), for the purpose of assessing blue mussels' size and density within the intertidal zone. To achieve this, several sub aims was set up to establish a workflow:

1. Capture images of quadrants covered with mussels and generate 3D models utilizing the SfM technique.

2. Conduct sampling of the mussels within the same quadrants to gather data on biomass and length distribution to generate biological metrics (BM).
3. Evaluate different complexity metrics (CM) to derive information about the surface complexity of each quadrant.
4. Establish a correlation between the selected CM and the BM

Once a workflow is established, it also enables integration of machine learning programs for object detection to further streamline the process.

2 Material and methods

2.1 Area of study and fieldwork

The study sites were located in the Hardanger fjord, close to the Hardanger bridge (Figure 2.1). The data presented and analysed in this thesis is based on photos and sampling from these sites. The sampling was conducted during low tide. If not, most of the mussels would be covered by water and collecting adequate photos would be challenging.

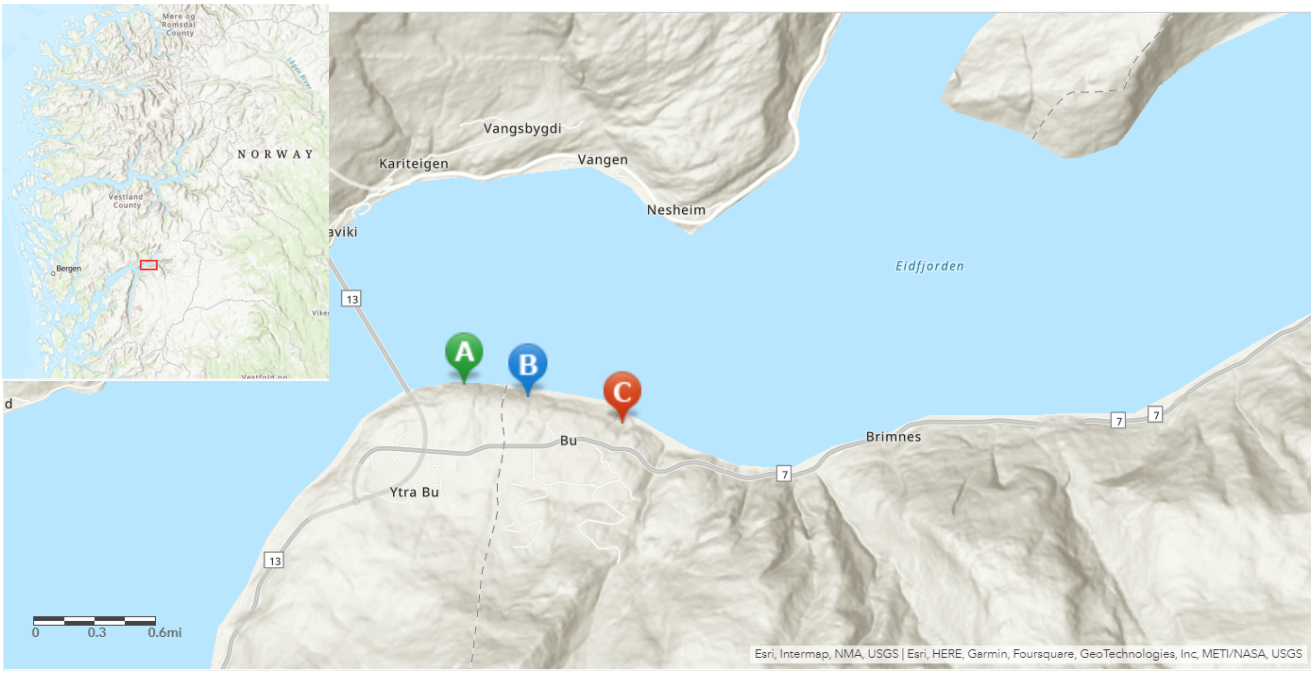

Figure 2.1. Map showing three study sites (A, B , C) where quadrants of mussels were collected and photographed. The map was generated with ArcGIS ArcMap.

Three sites which had continuous mussel coverage were chosen. Every study site in Hardanger fjord was reachable by boat. A diver swam from the boat to the site. The diver then placed a 0.4 m x 0.4 m quadrant several places at each site (Figure 2.2), which included a sample number and meter mark for reference purposes. Several overlapping photos of the quadrants were recorded using Olympus TG-6 and a Samsung SM-G78. The camera was positioned horizontally, directly over the quadrant, with at least 70 % overlap between images. There were 7-10 photos taken of each 0.4 x 0.4 m quadrant. The mussels within the quadrant were then scraped of the rock (Figure 2.3) and collected into a bucket for further analysis.

Figure 2.2: Placing the quadrants and scraping off the mussels within the quadrant.

Figure 2.3: Quadrants after the collection of mussels.

Due to poor weather conditions, we were not able to test the drone at the Hardangerfjorden location. However, a test with DJI Air 2s drone was conducted at several locations close to Austevoll. The drone was easy to manoeuvre, even from the boat, and the drone was used in manual mode to get as close to the rock as possible to get satisfying photos from each location. The manoeuvrability demonstrated by the drone exercise could indicate that capturing images under conditions similar to those used with traditional cameras is feasible. A transect of overlapping photos along the rocks with continuous mussels patches was created to test the photos from the drone and these were of high quality.

2.2 Sampling of biological metrics

The mussels from each quadrant was collected in buckets and total biomass for each quadrant was weighed. Each quadrant was then subsampled by splitting the mussels into equal parts, weighed again and each individual mussel were measured to obtain the length. Based on this information, the biological metrics was calculated (Table 6 in appendix). The mode, mean, and median mussel length for each quadrant was calculated using base R-studio functions (R Core Team, 2022). Biomass (g/m^2) and numbers/m^2 was calculated based on the numbers and weight of the mussels of each quadrant. Subsequently, a histogram was generated for each quadrant, demonstrating the length distribution of the mussels, as shown in Figure 5.1 in the appendix.

2.3 Models generation

Several 3D models from each quadrant were created using SfM techniques based on the 2D photos taken with an overlap of 80 %, which is recommended according to the Meshroom manual (Meshroom, 2021a). The photos recorded were loaded into Meshroom, a free open-source 3D Reconstruction Software (Figure 2.4).

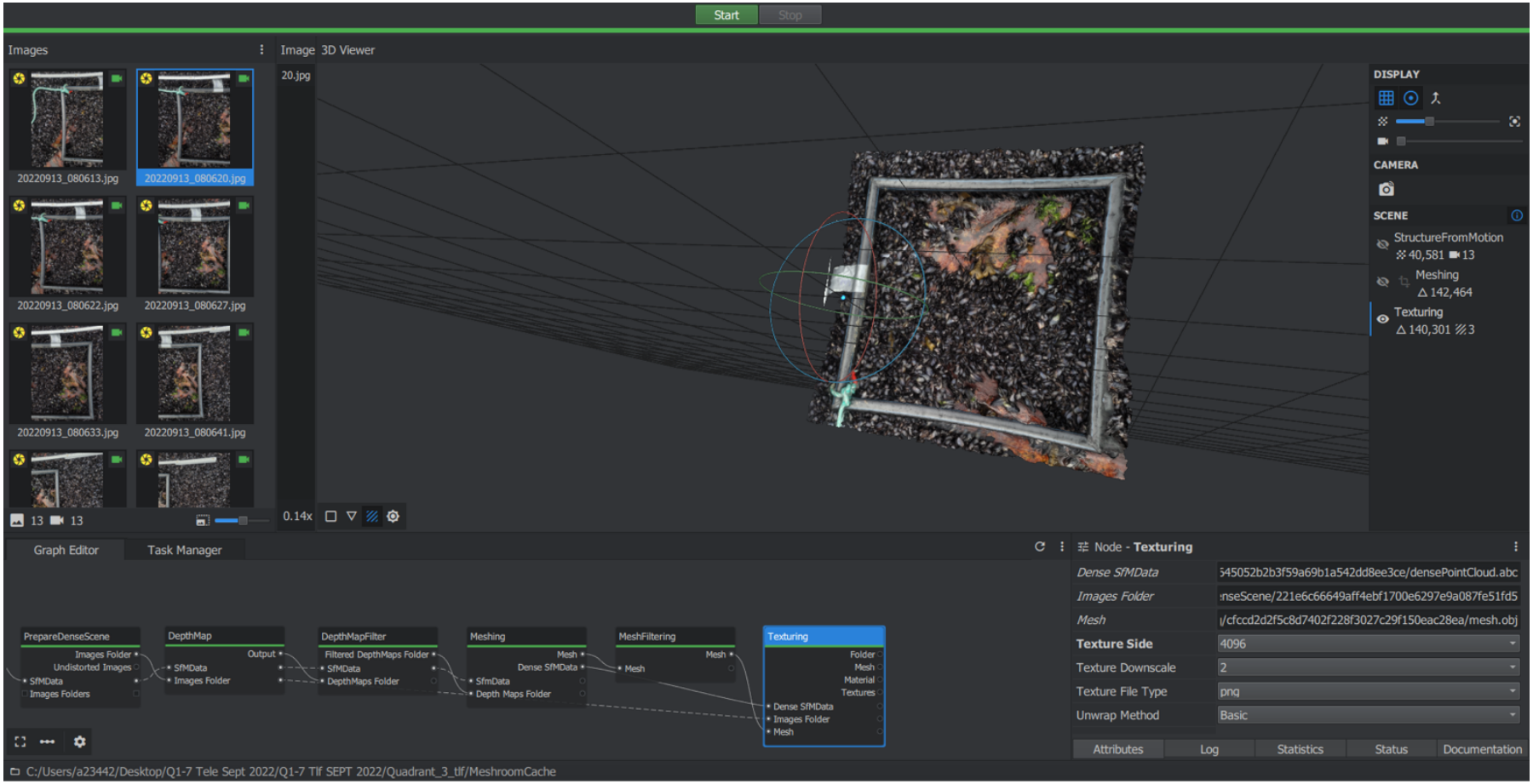

Figure 2.4: Screenshot showing the Meshroom workflow. In this example, the final node, "Texturing", is utilized as the concluding step to add texture to the model.

The initial phase involved importing images that overlapped from each quadrant into Meshroom, with each quadrant's project being saved separately. A basic workflow was followed using 5 different nodes, each possessing unique attributes (Meshroom, 2021a).

1) The first node to process was the "Structure-from-motion" node, which generates a point cloud symbolizing the exterior surface of an object, along with a representation of the diverse positions from which each photograph was captured.
2) If the initial results meet the expectations, the subsequent node, "Depth maps", is processed, selecting either 4 or 8 under "Downscale" to diminish the image sizes, thereby accelerating the computation speed.
3) The "Meshing mode" node was then utilized (Figure 2.5), which allows for the adjustment of the maximum number of points; in this instance, the limit was set to approximately 1.1 million points. Having a higher number of points will require more processing time, depending on the computers specifications. Also within this node, a "Custom Bounding box" was activated to constrain the computation to a specific area. In this scenario, the area encompassing the quadrant of mussels was selected.
4.) Upon the creation of the mesh, the "Keep only the largest mesh" option was enabled within the "Mesh filtering" node.
5) Lastly, the mesh was textured by computing the “Texturing” node, adding colour and detail to the 3D model (Figure 2.6).

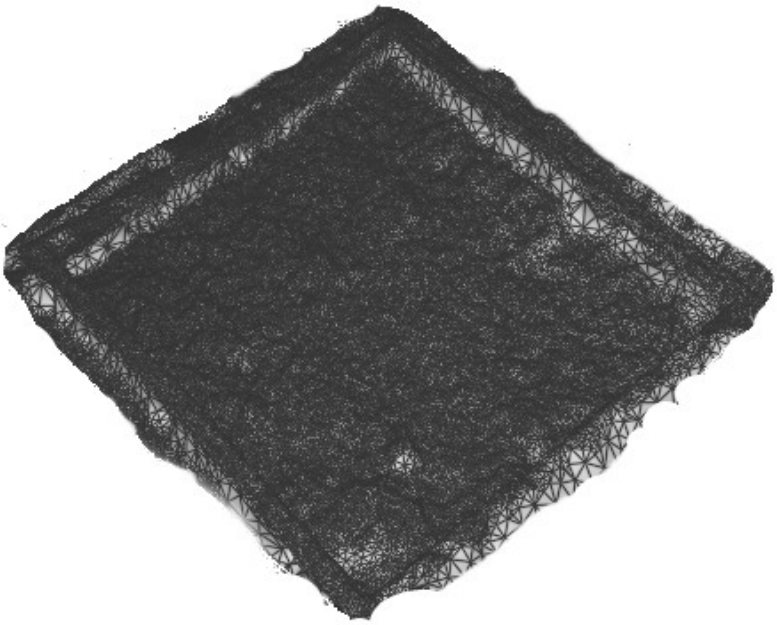

Figure 2.5: Mesh of the quadrant created in Meshroom after computing “Meshing mode”.

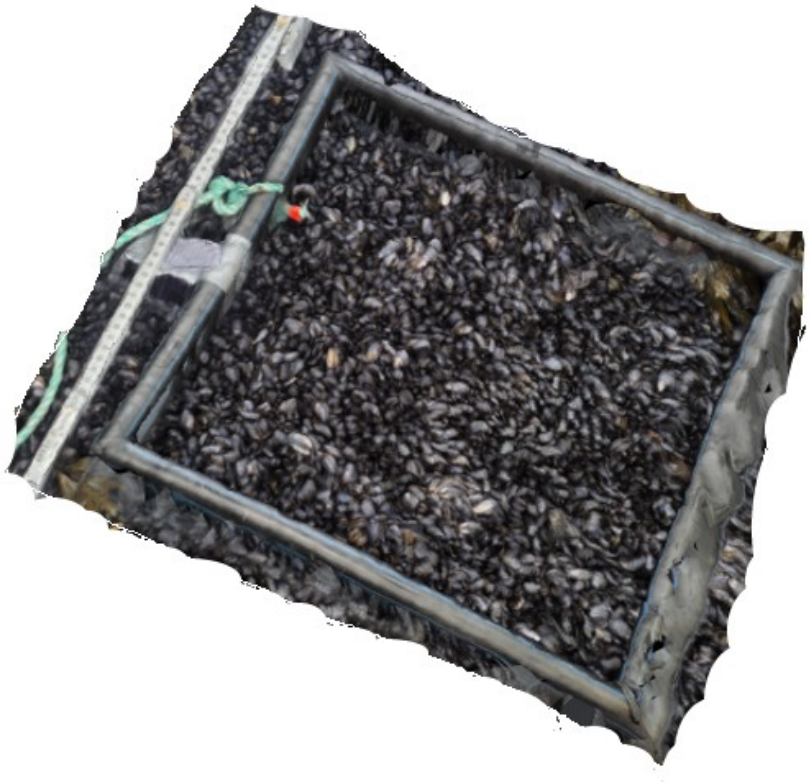

Figure 2.6: Final Textured 3D model from Meshroom, after colour and detail has been enhanced to the model.

Every step from the “Structure-from-motion” is automatically saved in in the mesh filtering subfolder of the Meshroom cache folder, so there is no need to further export it at the end of the process. The files needed for calculating CM were therefore loaded directly from the Meshroom cache folder.

2.4 Calculation of biological metrics

For all the quadrants biomass and abundance metrics were standardized to the area covered by mussels (AM) by dividing biomass and number of mussels with the area covered by mussels (1) and (2).

$$\frac{Biomass(g)}{AM} = g/m^2 \quad (1)$$

$$\frac{Numbers(n)\ of mussels}{AM} = n/m^2 \quad (2)$$

For quadrants that were entirely covered by mussels, the area (AM) equalled 0.16 m². In cases where the quadrants were not completely covered by mussels, the area occupied by the mussels within the quadrant was determined using the SketchAndCalc program (Icalc, 2020) . This was accomplished by sketching a polygon around the sections of the quadrant where mussels were present. The program was calibrated with the meter visible in the quadrant's photograph (as shown in Figure 2.5).

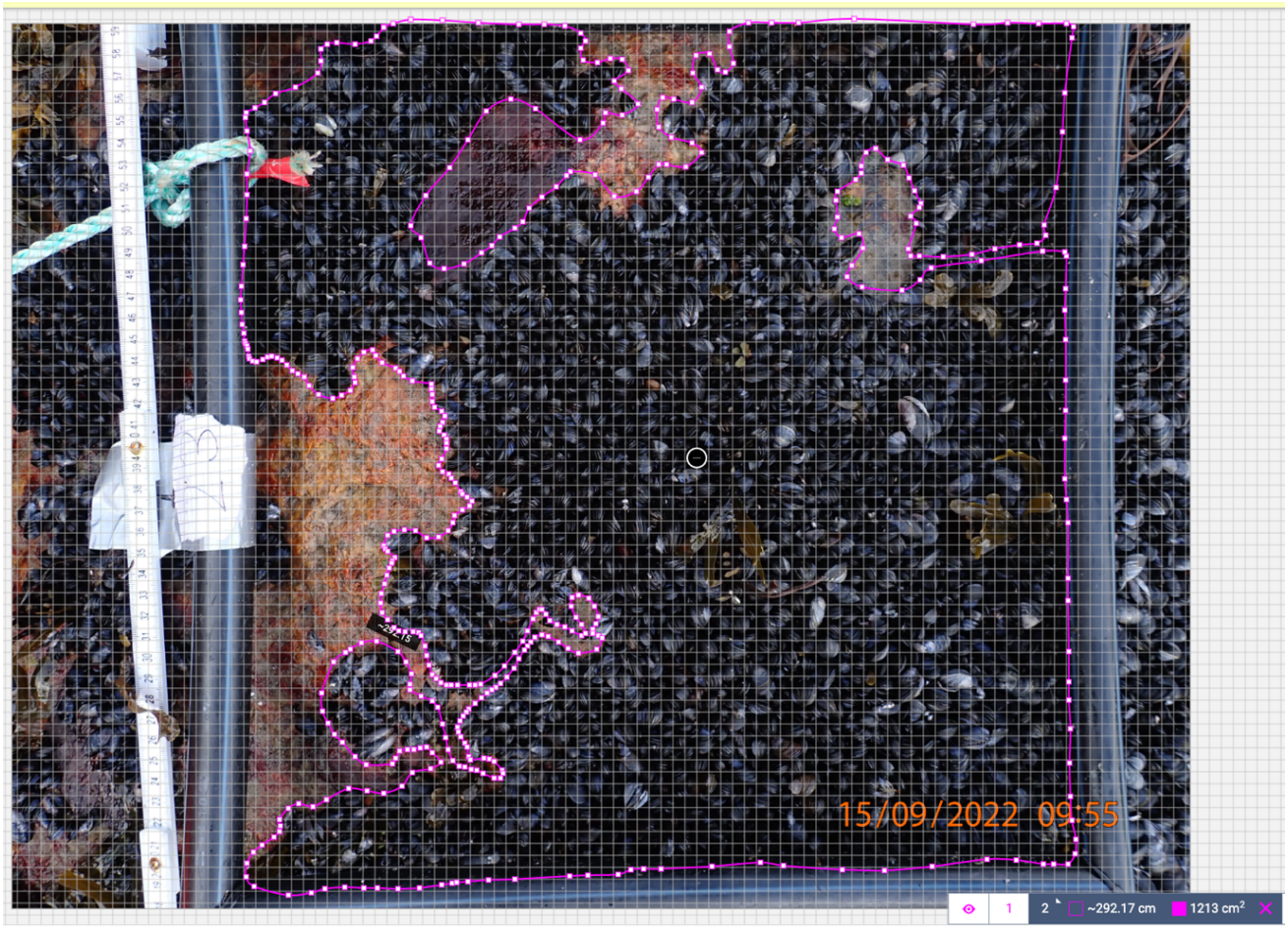

Figure 2.5: In cases where the quadrants were not completely covered by mussels, the proportion of the quadrant covered by mussels were calculated using SketchAndCalc.

2.5 Complexity assessment

The following analysis of the CM was then conveyed in Robert McNeels Rhinoceros 3D (McNeel, 2010). Rhino 3D is a 3D computer graphics and computer-aided design (CAD) application software and is a 3D modelling tool to improve product design. The textured model from MeshRoom was imported into Rhino 3D as a wavefront (.OBJ) file. The area selected for the complexity assessment was the area within the quadrant, and this area of the model was trimmed by creating a box with specific measurements using the "MeshTrim" function in Rhino. Three different CM were computed: rugosity, vector dispersion and fractal dimension. These metrics were calculated following the workflow described in Young et al., (2017) and by using the python scripts created by Young (2018). First, only the quadrants fully covered by mussels were analysed. To gather more data, quadrants with lower coverage were also subjected to subsampling and analysis. Sections corresponding to ¼ of the quadrants,

specifically those areas that had full mussel coverage, were chosen for subsampling. The CM for these sections were then calculated in the same manner as those for the fully covered quadrants.

Rugosity is a complexity metric commonly used in traditional coral reef research (Yanovski et al., 2017). It is typically computed in situ, by using the chain-and tape method, where a chain is positioned over a topography and the given length is then divided by the total length of the chain. To measure linear rugosity on a 3D model, a created mesh plane of twelve panels were intersected with the 3D model of the quadrant by using the function "MeshIntersect" in Rhino. The intersect created was then aligned and a custom python script for rugosity was run (Young, 2018), and following script asked to select the curves that were created based on the surface of the model. The output from the script gave the rugosity, as a result of calculating the length of the chain divided by the total length of the curve following the surface of the model. The output was given as rugosity for each curve, so for each quadrant, average and standard deviation were calculated.

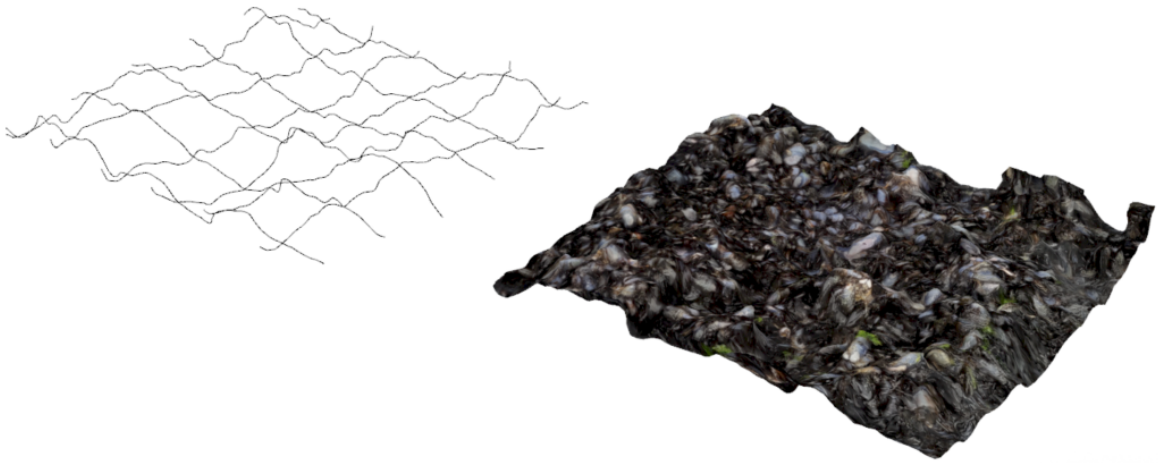

Figure 2.6: The figure to the right shows 0.4 x 0.4 m quadrant of the mussels and the figure to the left its respective transects used to calculate rugosity. The transects was created using Rhinosaurus 3D.

Vector dispersion (1/k) is considered to be an appropriate metric for measuring surface irregularity. It is defined as an estimate of vector variance for all individual surfaces considered (Carleton & Sammarco, 1987). Therefore, it measures the uniformity in angles of a surface. The output will be a value between 0 and 1, where 0 indicates a completely flat plane and the closer the value is to 1, the more complex the surface. This metric must be calculated at a certain resolution, and a 1 cm resolution was chosen, following the outline of Carleton & Sammarco (1987). Firstly, a planar "helper" surface was placed above the mesh of mussels, with the reef mesh positioned with one corner of the quadrant at the origin. Furthermore, to calculate this metric, a Python script for vector dispersion (Young, 2018) was run in the command section of Rhinosaurus 3D.

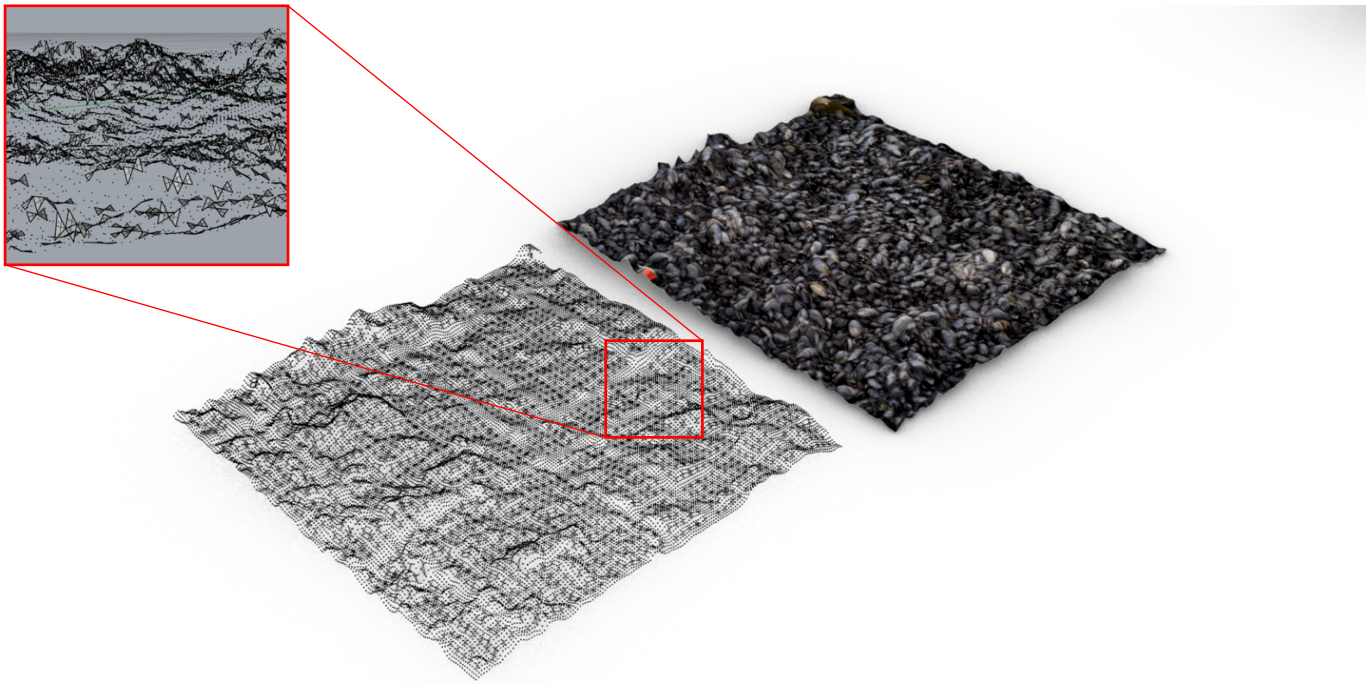

Figure 2.7: To the right, one quadrant (0.4 x 0.4 m) of mussels besides a grid of points spaced 1 cm apart to calculate vector dispersion.

The script created a grid of points with a prolific gauge over the physical surface, and the projected a grid of points, spaced 1 cm apart on the highest Z-point of the mesh. Then the script made triangles between each adjacent points and computed the directional cosines of triangles normal vectors. Lastly it computed 1/k using equations 3 and 4.

$$Q = \sqrt{(\sum_{l}^{i} cos_x)^2 + (\sum_{l}^{i} cos_y)^2 + (\sum_{l}^{i} cos_z)^2} \quad (3)$$

$$\frac{1}{k} = \frac{i - Q}{i - 1} \quad (4)$$

In these equations (3) and (4), *i* indicates the number of triangles created between surfaces points and cos_x, which is the directional cosine of a triangles normal vector in the x direction. Same applies for cos_y in y direction and cos_z in z direction. Like rugosity, average vector dispersion and standard deviation were calculated for each quadrant.

Fractal dimension (FD) was chosen as a complexity metric because it is regarded as an accurate and sophisticated measurement to assess surface complexity. It has been shown to be suitable to describe the complexity of coral reefs (Bradbury & Reichelt, 1983) and could therefore also be well suited to assess the complexity of the surface of mussels beds. The method was developed based on the idea of mathematician Benoit Mandelbrot (Mandelbrot, 1983). It gives a value for a surface between 2 and 3 where a larger value indicates greater complexity. The resolution used to calculate fractal dimension can vary based on the objective of the research, for example defining the resolutions to get information about a specific species and its distinctive habitat requirements. In this case, fractal dimension is used to acquire as much information as possible about the surface within the quadrant, therefore multiple intervals were chosen.

FD reveals how the area of a surface changes with resolution. This describes the relationship between the resolution of a model and its surface area. The surface area will increase with finer resolution (Young et al., 2017). The resolutions (δ) used in this study were 17.5 cm, 35 cm and 70 cm. To acquire FD, another python script was used on the quadrants in Rhinosaurus 3D (Young, 2018). Necessary alterations of the script were done to get desired resolutions for each quadrant. The script for FD re-rendered the model at the given resolution δ by putting a grid spaced at δ onto the model, almost like dropping a blanket on it. The script then connected

adjacent points and formed a new surface that was plotted against δ on a logarithmic scale and the slopes between points were determined.

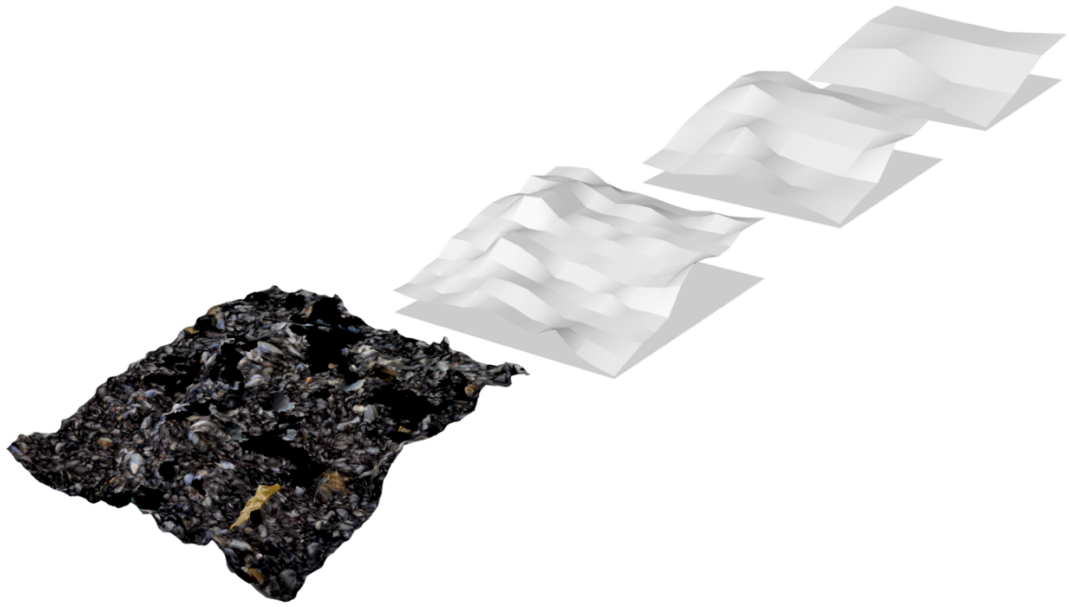

Figure 2.8: Fractal dimension for different resolutions (17.5 cm, 30 cm and 70 cm) for a quadrant of 0.4 m x 0.4 m. Generated with Rhinosaurus 3D.

2.6 Accuracy assessment

A meter was positioned adjacent to each quadrant, serving as a reference point. This was to assess the accuracy of the 3D models created by Meshroom before the model was trimmed to only the 0.4 x 0.4 m area within the quadrant. Using the meter as a reference point, the length from each edge of the quadrant, which was positioned on the mussel beds, was determined to be 44 cm wide. To do the measuring, the OBJ. file from the 3D models was imported into a program called Meshlab (Meshlab, 2022). After some calibration of the program, it was possible to measure distances on the 3D model. The relative error of the constructed 3D model, was estimated by dividing absolute difference between model length (ML) minus the actual length (AL) that is known divided by actual length (5).

$$Accuracy = \frac{|ML-AL|}{AL} \quad (5)$$

2.7 Augmentation method

To extract more information and better assess the variability of complexity metrics from each full quadrant, an augmentation technique was used to increase the number of replicates. Each quadrant was divided into four smaller quadrants and the CM were extracted from each quadrant. This resulted in different metrics but all of them corresponded to the same biological data that was recorded for the full quadrant.

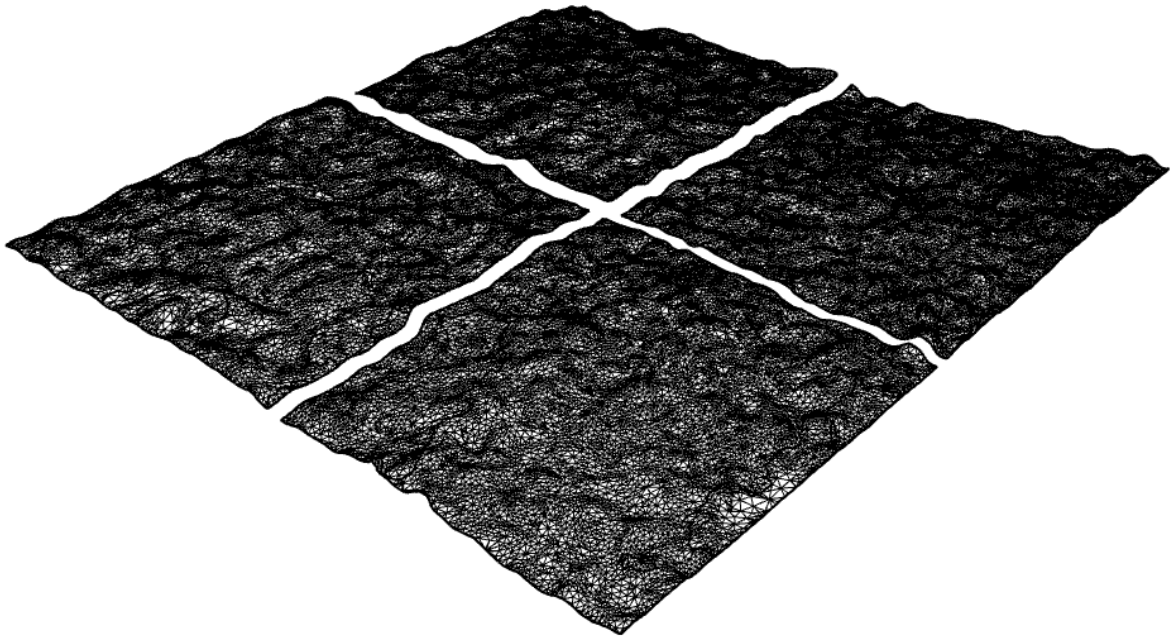

Figure 2.10: A quadrant with full coverage divided into four smaller quadrants to calculate complexity metrics for each of them .

2.8 Model of Workflow

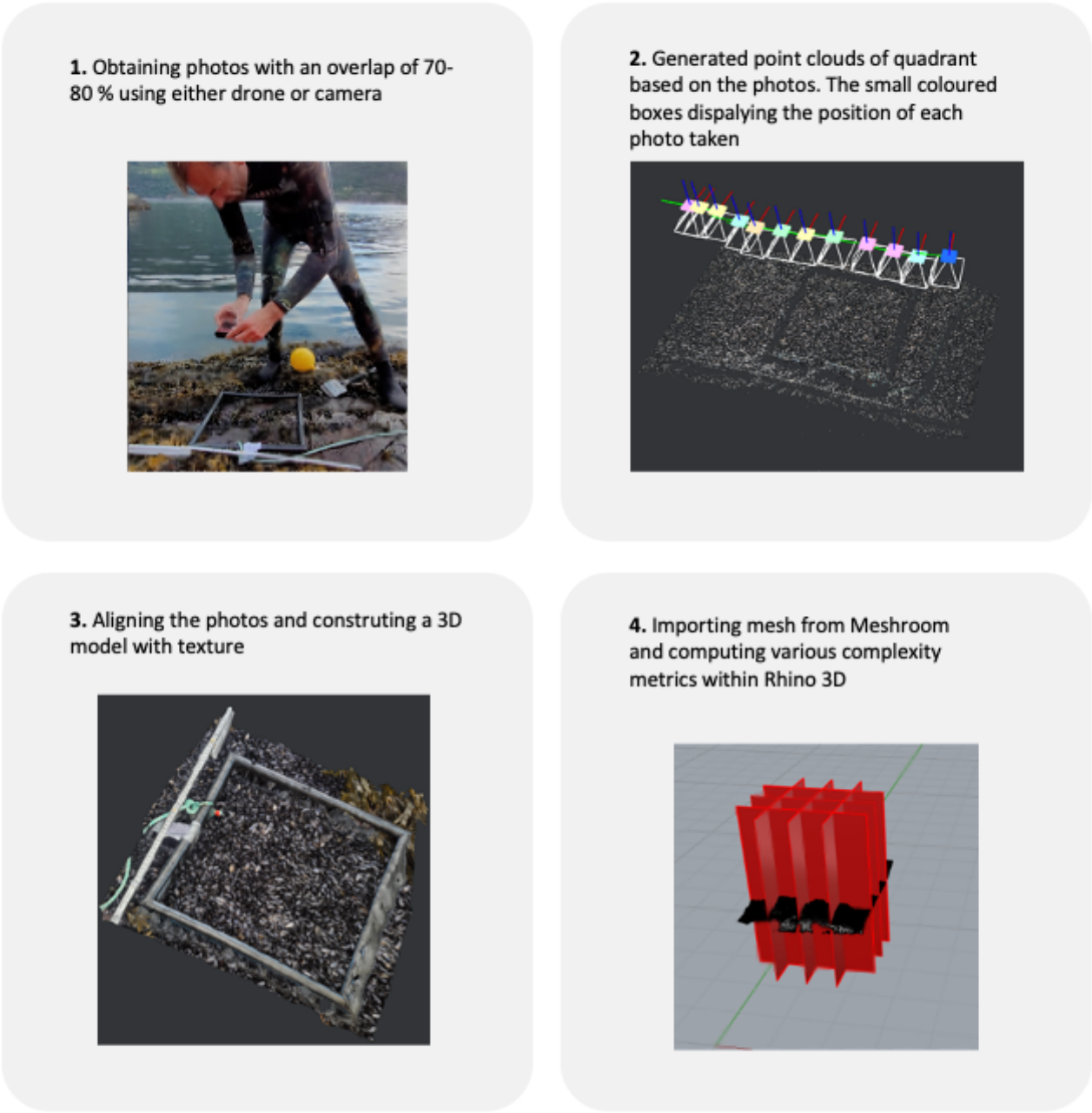

Figure 2.9: Workflow of the collection of complexity metrics using Meshroom and Rhinosaurus 3D.

2.9 Statistical Analysis

A correlation analysis was utilized to explore the relationships between the CM and the information provided by the BM. All the analysis were conducted using R (R Core Team, 2022). First, a correlation analysis was performed to determine whether there was a linear relationship between the BM (biomass/m^2, numbers/m^2, median, mode, mean) and the complexity metrics (fractal dimension, vector dispersion, and rugosity). Normally, Pearson correlation would be used in this situation, but a Spearman rank correlation was chosen instead because some of the metrics did not exhibit normal distribution (as demonstrated by visual inspection of the variable histograms (Figure 5.2 in Appendix) and a Shapiro-Wilks test, presented in the "Results" section). Spearman rank correlation is a non-parametric measure of association, which means it does not presuppose a certain data distribution. It gauges the monotonic relationship between two variables, which may or may not be linear. Spearman correlation is less susceptible to outliers because it is based on the ranks of the data rather than the actual values.

Due to the Spearman ranked correlation showing a weak linear relationship between the CM and BM but high correlation separately between those two group of variables, a principal component analysis (PCA) of each of the group was conducted in order to reduce the dimensionality of the data. By generating new vectors called principal components, PCA aids in reducing the number of dimensions while preserving as much information as possible. These elements are unrelated to one another and are linear combinations of the initial variables. It was simpler to visualize the data in a scatterplot when the dimensionality of a dataset was reduced. This made patterns, clusters, or outliers visible that were not initially visible in the high-dimensional space.

To assess the potential of the complexity metrics PCs (Principal Components) in describing the biological metrics a principal component regression (PCR) was used. PCR is a technique that combines PCA and linear regression, and can be useful when there is a large number of predictor variables that may be highly correlated. Firstly, the explained variance of each PCs was determined by creating a cumulative variance plot. An appropriate number of PCs was chosen to explain a significant number of the total variance while balancing the trade-off between model complexity and explained variance. The optimal number of PCs was selected using cross-validation, to mitigate the problem of overfitting. It involves partitioning the data

set into subsets, then estimating the model on one subset (called the training set) and validating the model on the other subsets (called the validation set). Subsequently, you get the Root Mean Square Error of Prediction (RMSEP), which serves as a measure of the discrepancies between the model's predicted values and the actual observed values. In addition, you receive the Adjusted Coefficient of Variation (adjCV). This metric considers the sample size, offering a more precise gauge of dispersion, especially for smaller sample sizes. The selected PCs based on the CM were applied to the different BM as the response variable. The model was fit to the data to obtain the regression coefficients and the R- squared (R^2) of every linear regression. R^2 is a measure of how well the regression predictions approximate the real data points. Every linear regression was checked for normality using a QQ plot to check the assumption of normality for the residuals. An R^2 of 100 percent indicates that all changes in the dependent variable are completely explained by changes in the independent variables.

The use of PCR therefore helped to address, multicollinearity issues, reduced noise and improved interpretability. Some of the PCs explain a considerable part in describing the variance in the data and they are therefore further investigated in order to identify which CM variable contributes the most to those PCs. To further look into the relationship between the CM and BM, a canonical correlation analysis (CCA) was conducted to provide additional insights into the correlation structure of the datasets. This analysis may reveal more complex or subtle relationships between the two datasets, given the fact that CCA can capture multivariate correlations that are not detectable by univariate correlation measures or by PCA, which only considers one dataset at a time. CCA, in contrast, finds linear combinations of the variables in each dataset that are maximally correlated with each other. The canonical correlations, which have a range of -1 to 1, express how closely each pair of canonical variates is related. The first pair is determined in such a way as to maximize the correlation between the two sets of variables. The second pair is computed under the constraint that it is uncorrelated with the first pair, and so on for subsequent pairs. The pairs are therefore ordered by the amount of shared variance they explain, with the first pair explaining the most, the second pair the second most and so on. The canonical pairs showing a high correlation were further examined by looking into their coefficients to identify which variables of the original datasets that contributed most to these relationships.

3 Results

3.1 Exploring the distribution of complexity and biological metrics

A total of 4316 mussels were measured by length. There was a large difference in the size distribution between the quadrants with a mean value for each quadrant ranging from 6.6 mm to 23.8, and with a mean value for the total of mussels of 10.41 mm. The examined mussels in this study represent the smaller half of the species' full size range with the total mussels having a size range of 63 mm and a mean length of 10.41 mm. The biological metrics are illustrated in Figure 3.1a, with numbers/m^2 and average weight per mussel(g) displaying notable outliers.

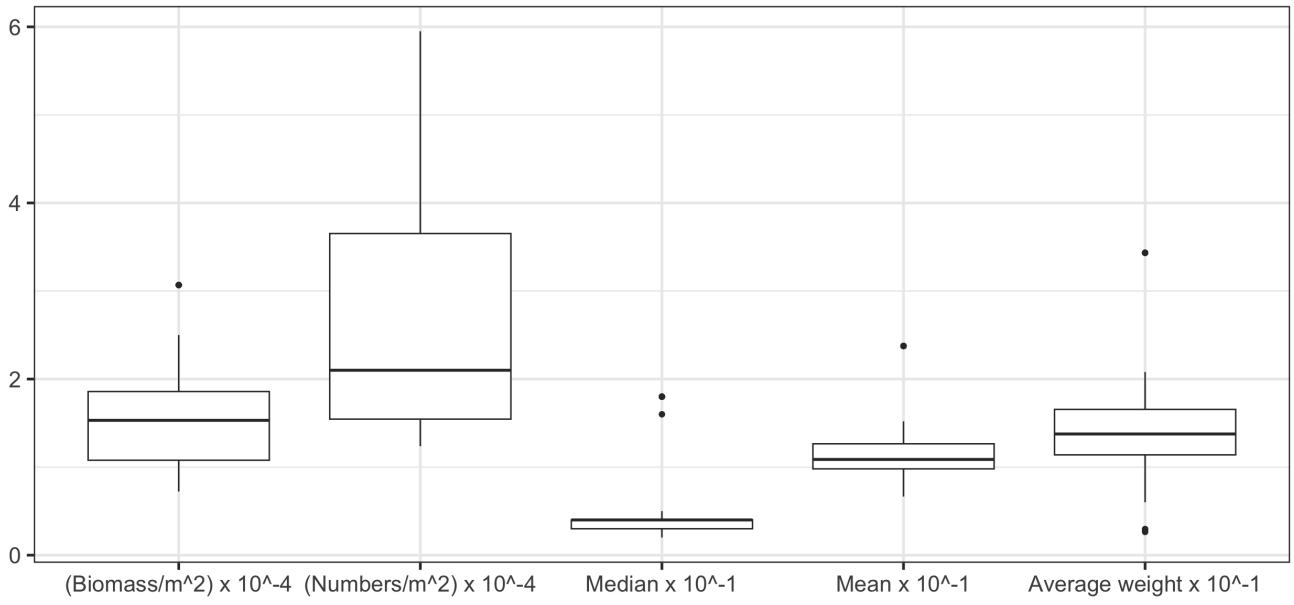

Figure 3.1a : Boxplot of biological metrics ((biomass(g)/m^2) x 10^{-4} , (numbers/m^2) x 10^{-4}) , median(mm) x 10^{-1}, mean(mm) x 10^{-1}, average weight per mussel(g) x 10^{-1}).

Boxplots presenting the distribution of the complexity metrics revealed some substantial outliers among the metrics, in particular for vector dispersion (Figure 3.1b) and fractal dimension (Figure 3.1c).

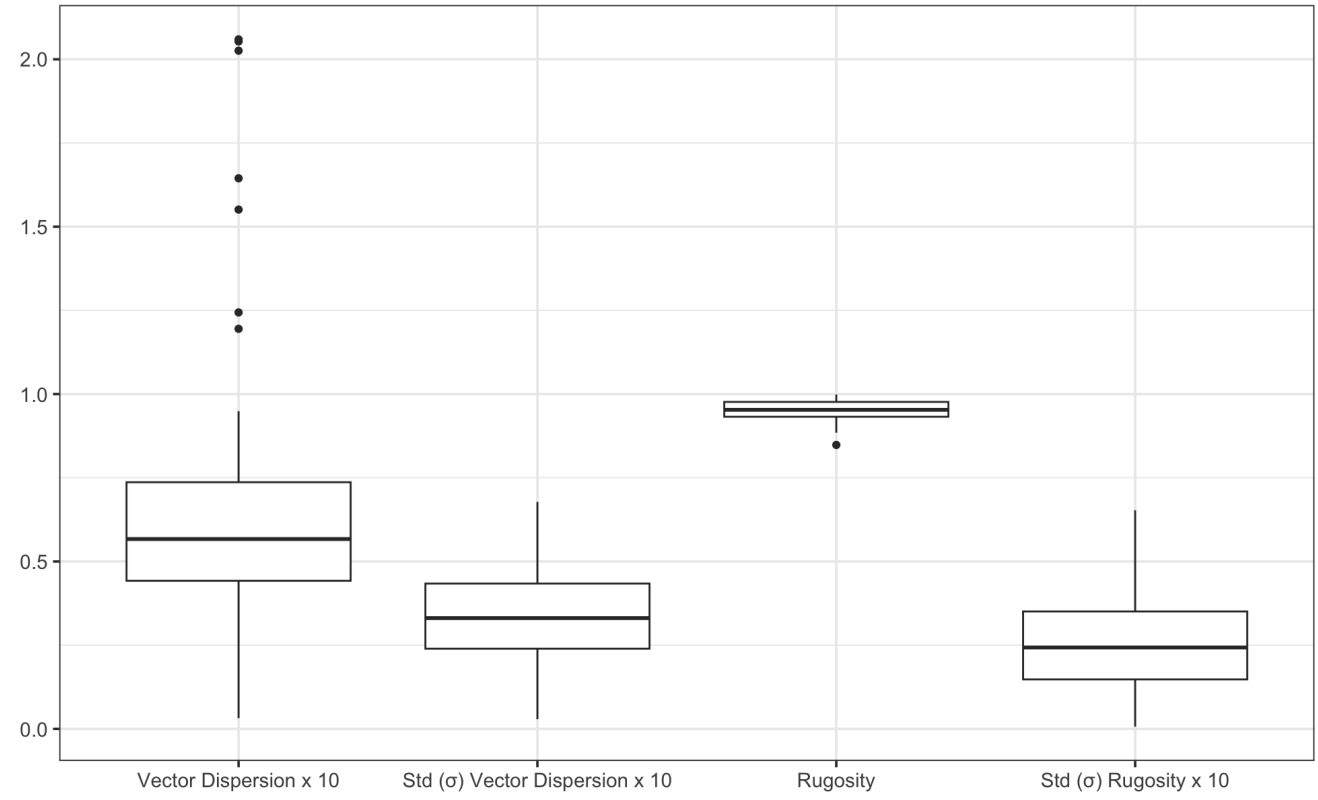

Figure 3.1b : Boxplots of complexity metrics (vector dispersion x 10, Std(σ) vector dispersion, rugosity, Std (σ) rugosity) for every quadrant.

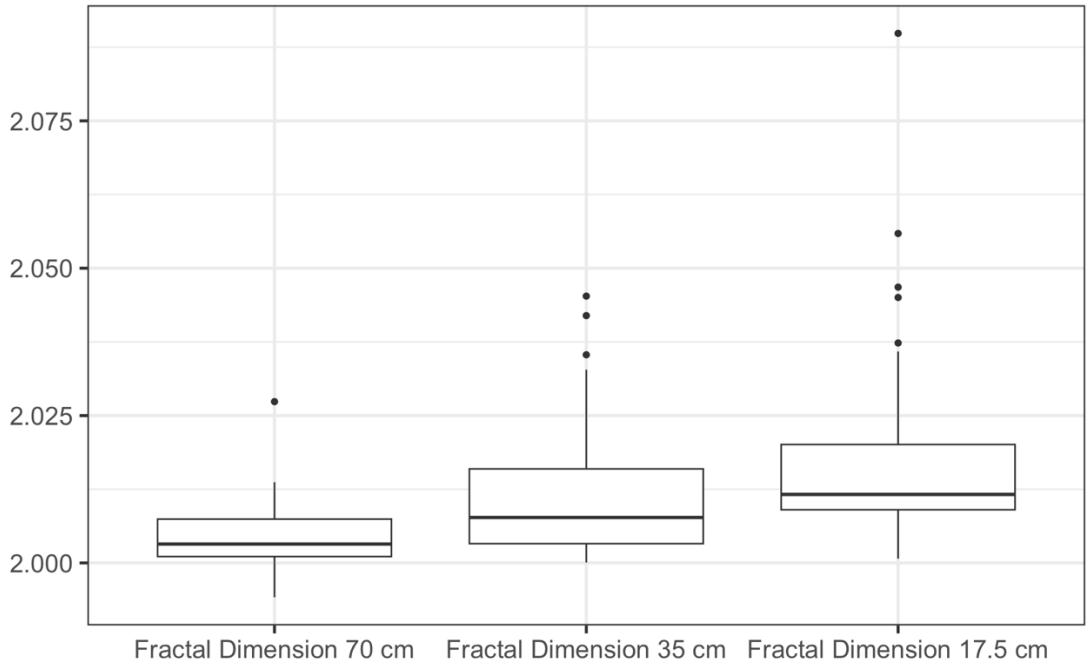

Figure 3.1c: Boxplot of complexity metrics (fractal dimension 70 cm, fractal dimension 35 cm, fractal dimension 17.5 cm).

3.2 Correlation analysis

According to the Shapiro-Wilkins test (Table 1 & 2) and visual interpretation of the histogram plot (Figure 5.1 in appendix), most of the variables had p-values that were lower to the selected significance level (P 0.05), indicating that they did not have a normal distribution.

Table 1: Shapiro-Wilks test (significance level p) for complexity metrics : vector dispersion (VD), vector dispersion standard deviation (VD SD), rugosity, rugosity standard deviation (SD), fractal dimension (FD) (70 cm , 35 cm, 17.5 cm)

	VD	VD SD	Rugosity	Rugosity SD	FD 70 cm	FD 35 cm	FD 17.5 cm
p-values	3.78e-06	6.99e-01	3.70e-02	2.20e-01	2.49e-05	5.20e-06	1.35e-07

Table 2: p-values from Shapiro-Wilks test for biological metrics.

	Biomass/m^2	Numbers/m^2	Mode	Mean	Median	Weight Per Mussel
p-values	7.45e-04	4.03e-05	7.44e-12	1.69e-08	3.52e-08	2.88e-05

The Spearman rank correlation found a poor correlation between the variables from the two groups (CM and BM), but a substantial correlation within each group (Figure 3.2). This indicates a weak linear relationship between CM and BM. However, biomass (g/m^2) was an exception, and the correlation coefficients (ρ) was 0.73 and 0.70 with fractal dimension 35 cm and vector dispersion SD respectively (Figure 3.2).

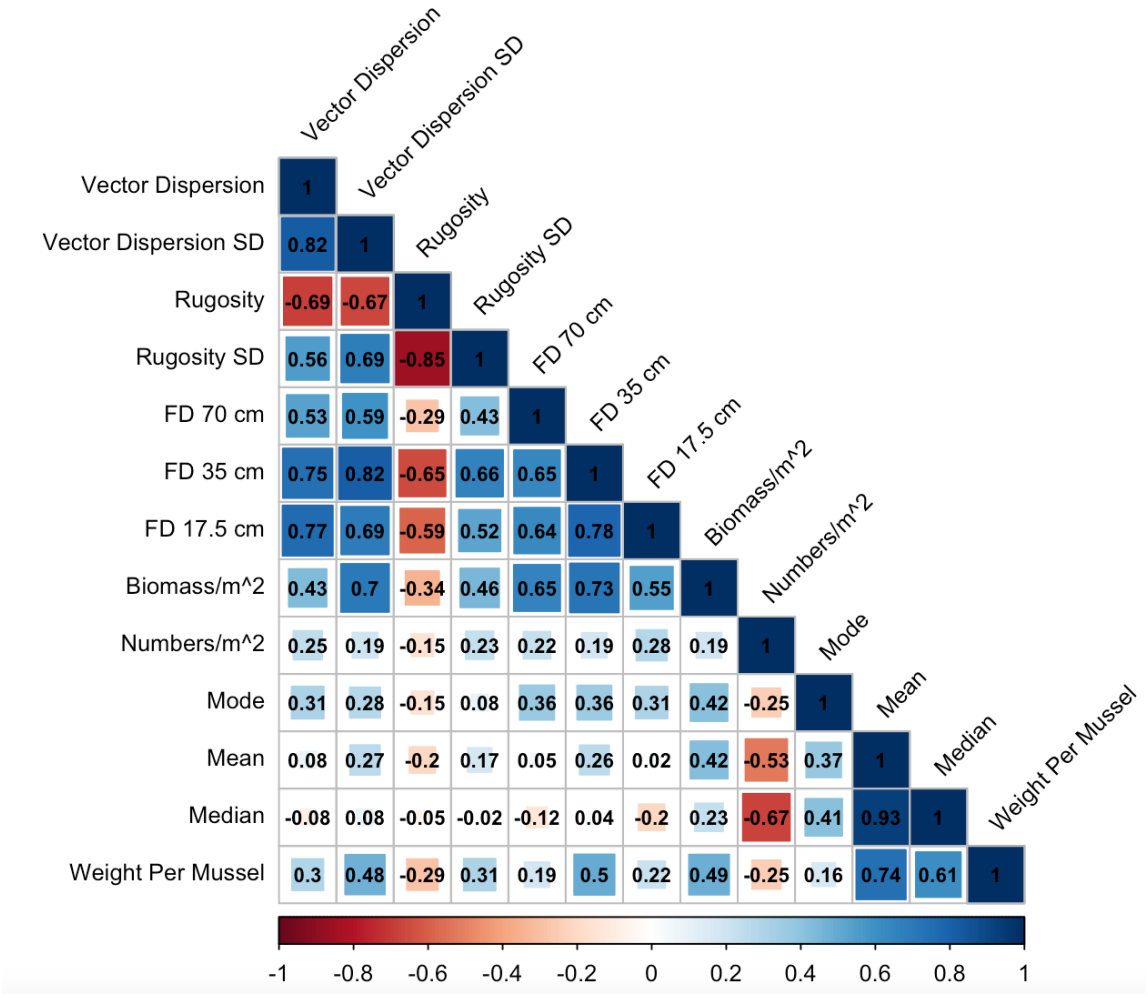

Figure 3.2: Spearman Ranked Correlation demonstrating the strength and direction between biological and complexity metrics.

3.3 Principal Component analysis

The cumulative explained variance plot for the PCs based on CM and BM was created to determine the relative importance of each PC (Figure 3.3a and Figure 3.3b). PC1 (68.32 %) and PC2 (11.44 %) explained 79.76 % of the variance for the PCs of the CM. PC1 (59.09 %) and PC2 (23.65 %) explained 82.74 % of the variance for the BM.

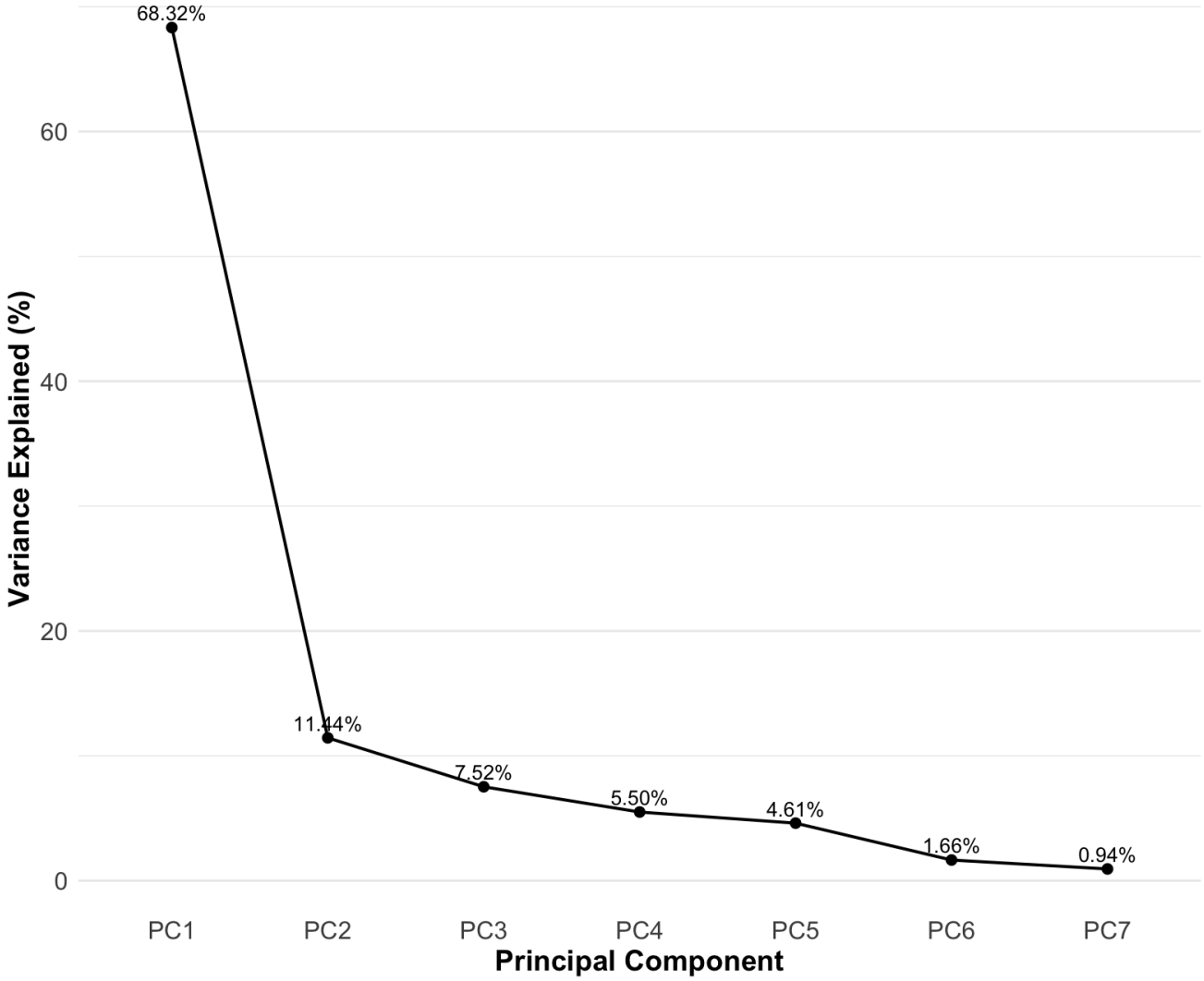

Figure 3.3a: Cumulative variance explained (%) for each PC created from the complexity metrics.

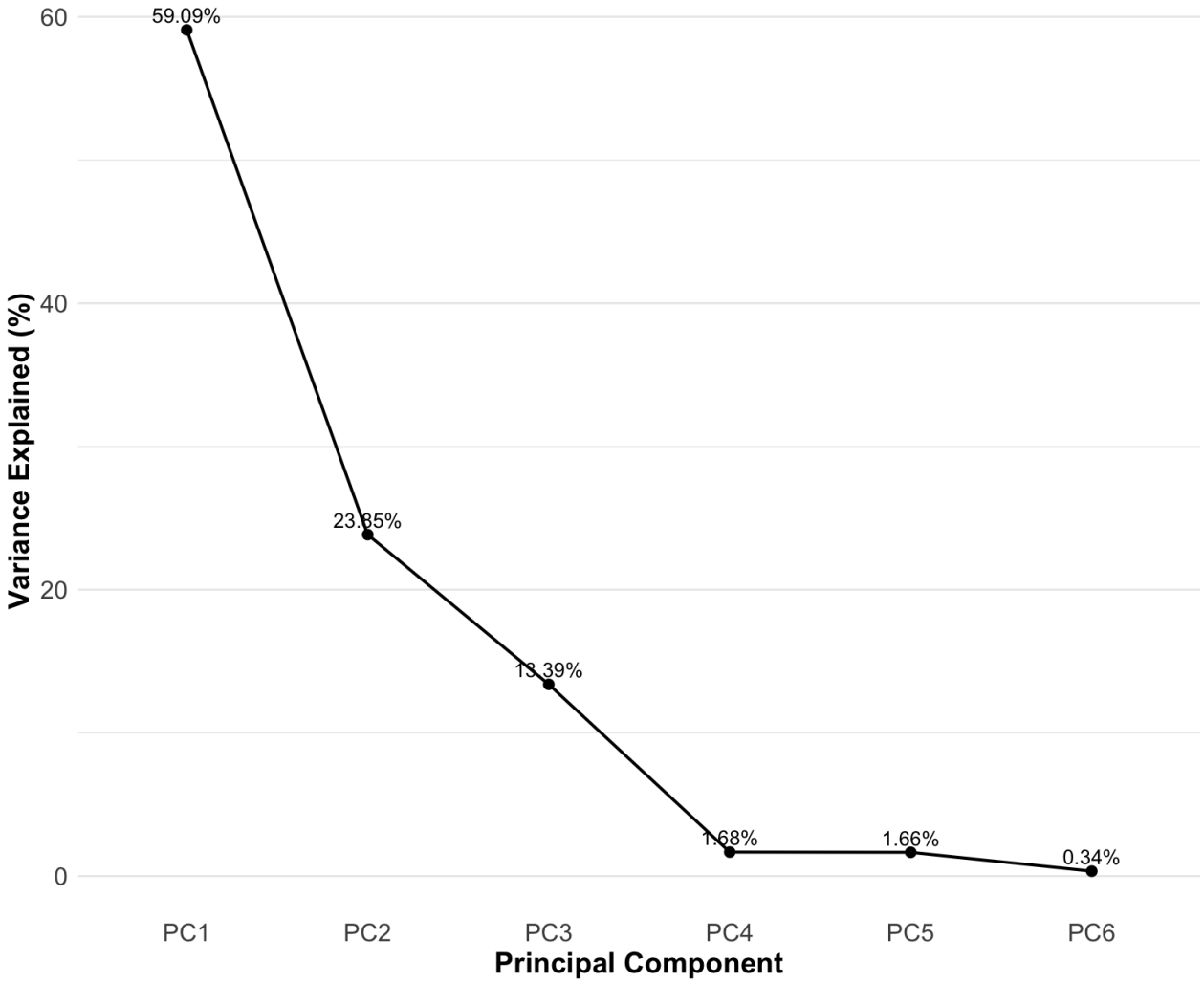

Figure 3.3b: Cumulative variance explained (%) for each PC created from the biological metrics.

The PCA plot was made with the CM (Figure 3.4a) for the two first PCs and displayed no clear grouping and one defined outlier. Rugosity and rugosity standard deviation displayed a strong negative correlation while both fractal dimension (FD) and vector dispersion was grouped together.

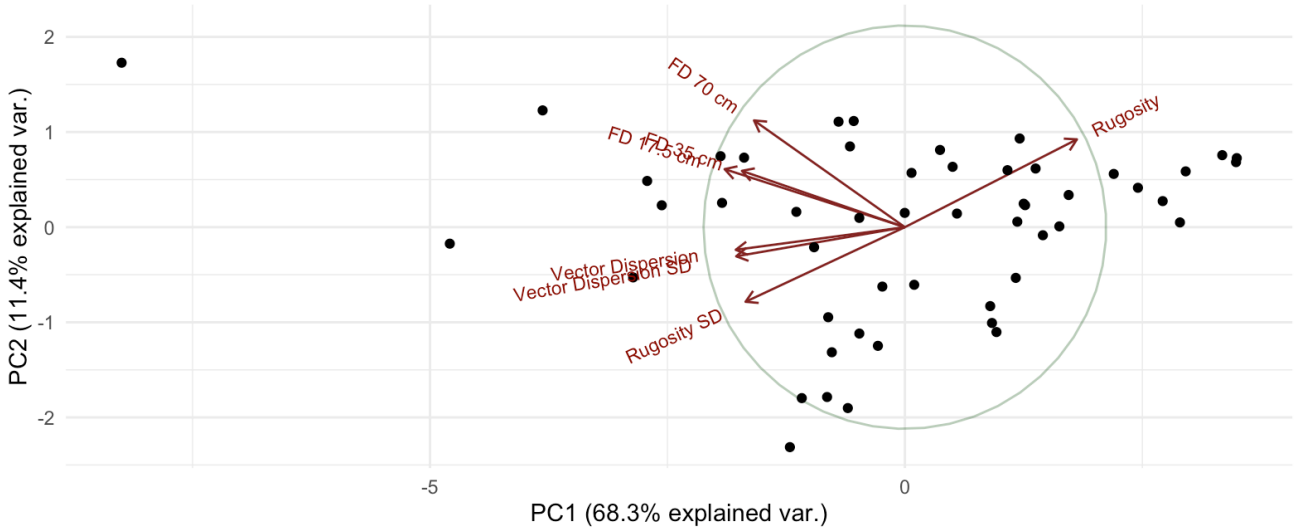

Figure 3.4a: PCA of complexity metrics.

The same plot was created for the BM (Figure 3.4b) and did also not display any grouping. However, mode, median and mean displayed a strong negative correlation with Numbers/m^2.

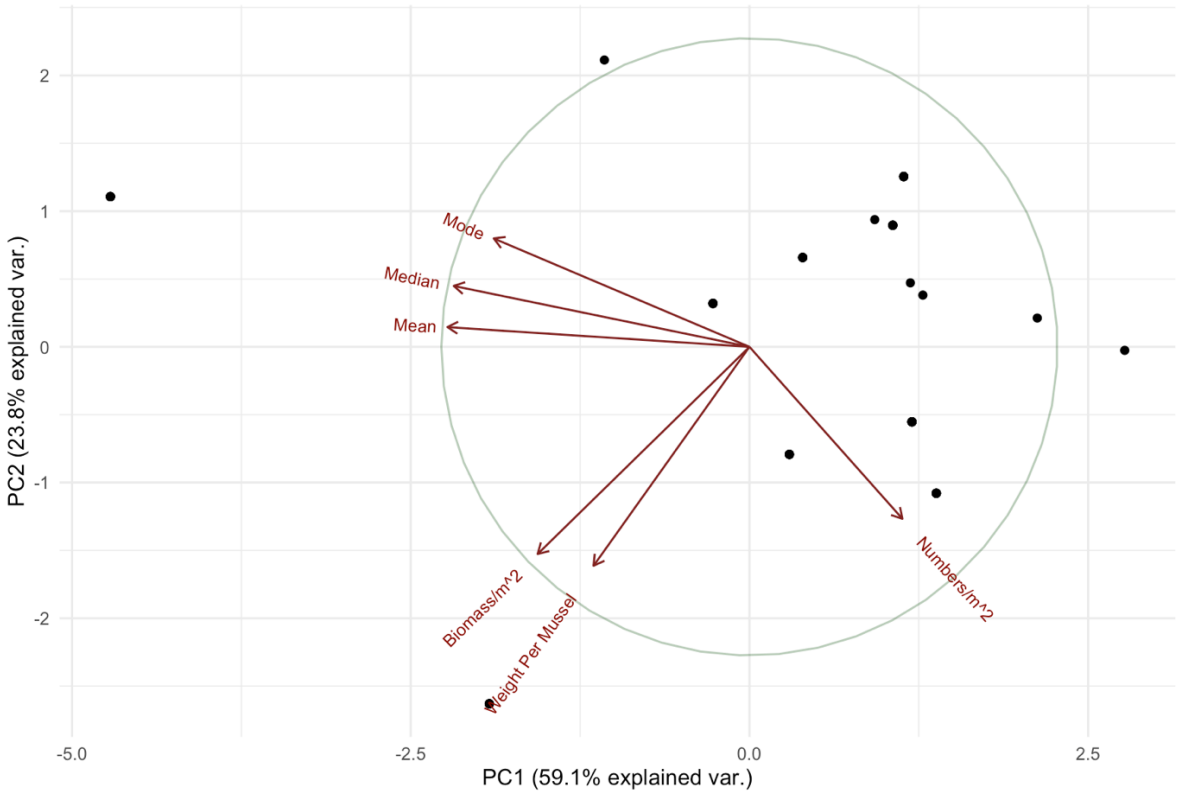

Figure 3.4b: PCA of biological metrics.

3.4 Principal Component Regression (PCR)

Cross-validation (CrV) revealed that five components (PC1–PC5) offered the best prediction for the response variable with the smallest Root Mean Squared Error of Prediction (RMSEP) and adjCV (Table 3).

Table 3: Root Mean Squared Error from the Cross-validation. Intercept describing the baseline of the model without any PCs.

	Intercept	1 comps	2 comps	3 comps	4 comps	5 comps	6 comps	7 comps
CrV	6917	6276	6521	6748	6390	5385	5442	5454
adjCV	6917	6261	6503	6795	6190	5338	5396	5393

PCs 1 through 5 were used to identify any underlying patterns in the data. Table 4 describes the R^2 for each linear regression from the biological measurements as the response variable and a new selection of PCs produced from the CM as the predictor variables. Every QQ plot indicated that the residuals were normally distributed. Biomass and weight per mussels had the highest R^2, with biomass for PC1-PC5 having an R^2 of 0.5416.

Table 4: Displaying R^2 for different combinations of PCs against the biological metrics, with the largest values highlighted.

	Biomass/m^2	Numbers/m^2	Mode	Mean	Median	Weight per mussel
R^2 (PC1)	0.2112	0.0587	0.006752	0.0114	0.001171	0.1077
R^2 (PC1-PC2)	0.2172	0.0587	0.05317	0.0372	0.004021	0.1078
R^2 (PC1-PC3)	0.2497	0.06857	0.05411	0.0377	0.005765	0.113
R^2 (PC1-PC4)	0.4702	0.07422	0.07797	0.1532	0.08633	0.3438
R^2 (PC1-PC5)	0.5416	0.08074	0.08024	0.1636	0.09981	0.3522

Plots displaying the linear relationship for the usually most determining PCs (PC1 & PC2) against the variables of the biological variables is illustrated in figure 3.5a and figure 3.5b. The plot with PC1 presented mostly a negative correlation, in particular with biomass/m^2 and weight per mussel which corresponds with R^2 from table 4. The linear regression plot for PC2 shows a weak correlation with most of the BM. However, the linear regression plot for PC4 (Figure 3.5c) showed a stronger positive correlation with the BM.

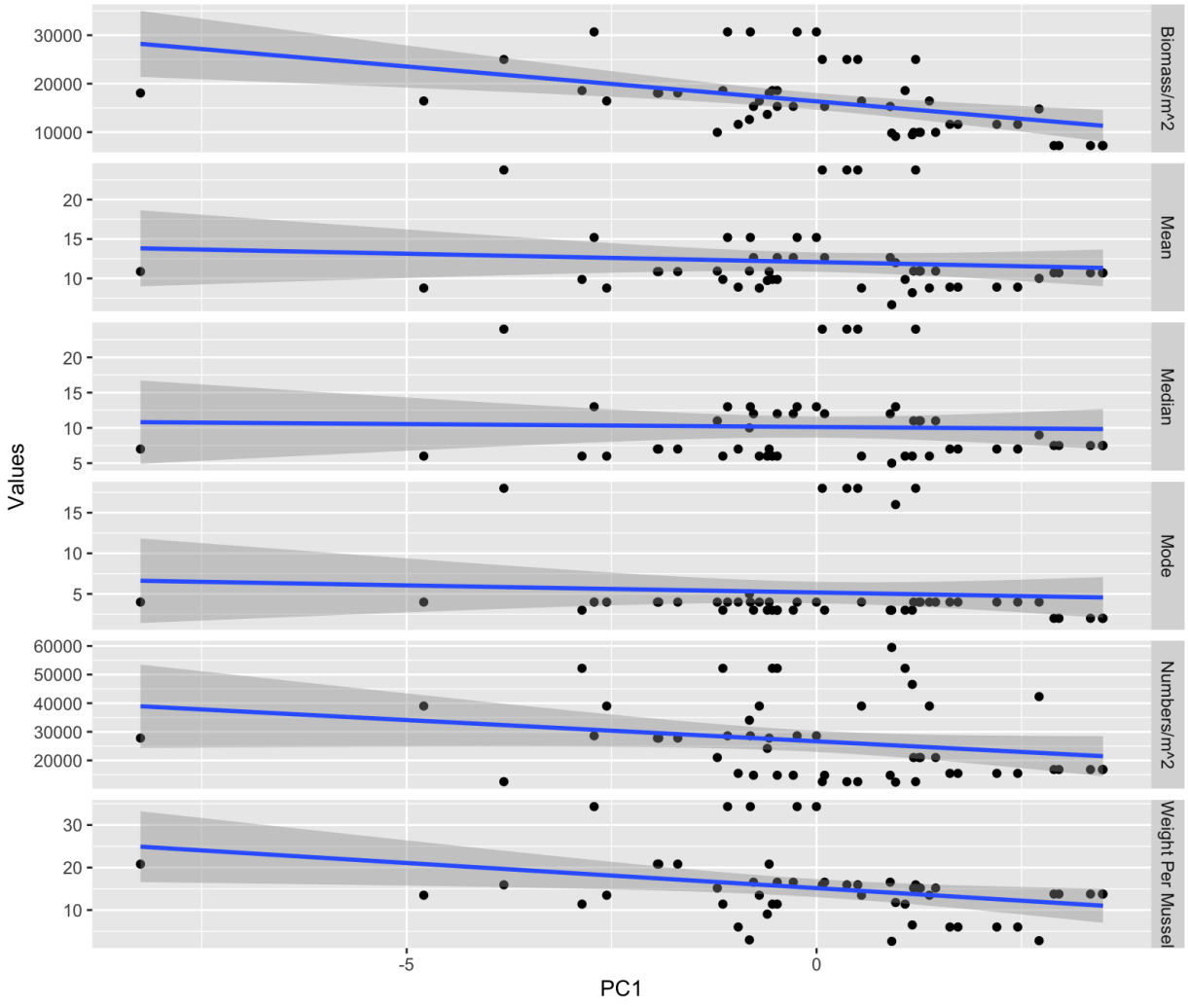

Figure 3.5a: Linear regression for each variable against PC1.

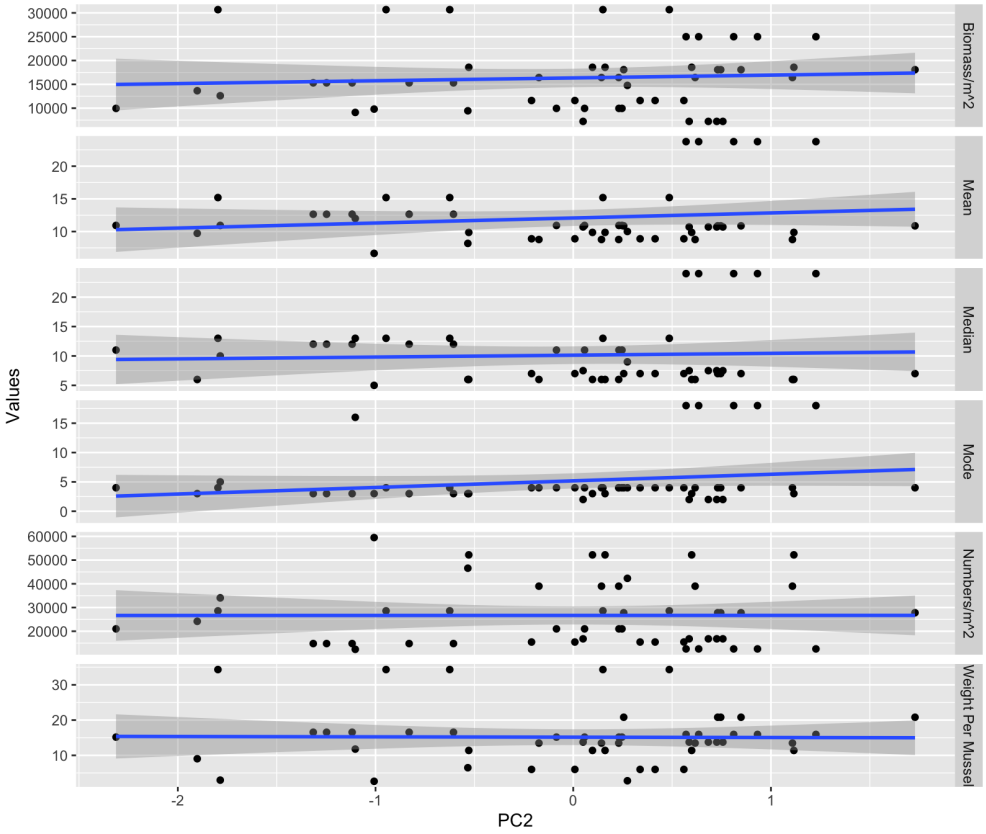

Figure 3.5b: Linear regression for each variable against PC2.

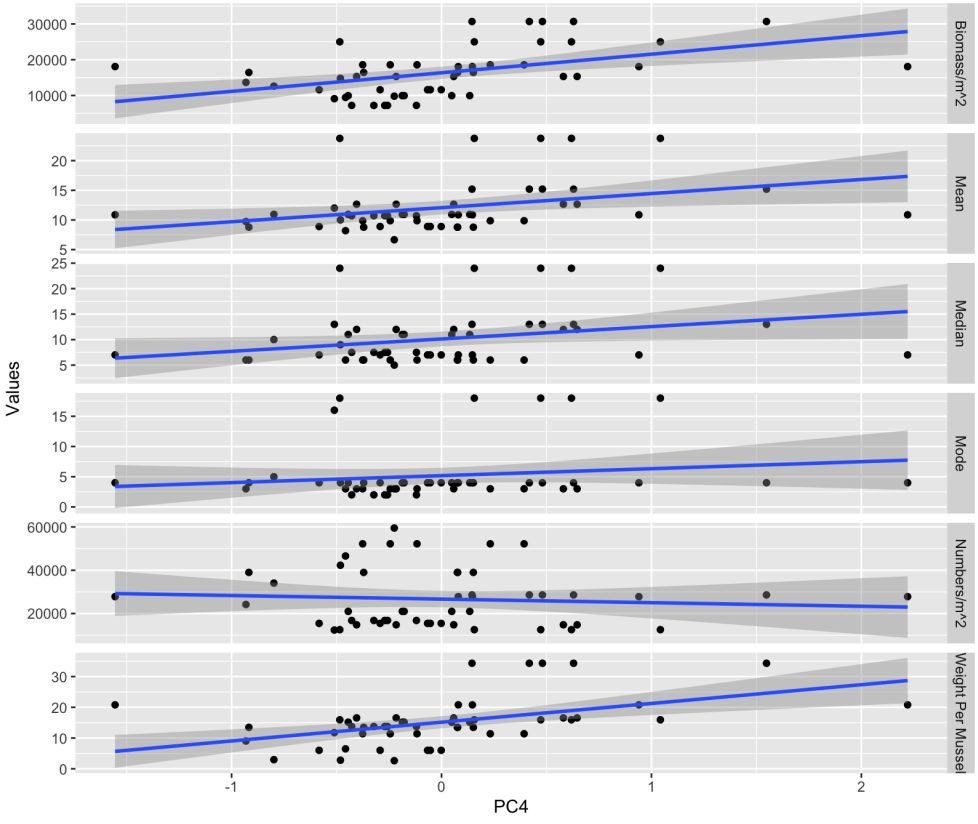

Figure 3.5c: Linear regression for each variable against PC4.

PC1 and PC4 explains a substantial part of the variance in the data and it is therefore further investigated in order to identify which variable contributes the most. The variable of FD 17.5 cm (Figure 3.6a) contributes most to PC1, however, there is a quite similar contribution to PC1 for each variable. PC4 on the other hand, has a substantial contribution from FD 35 cm and Vector Dispersion SD (Figure 3.6b)

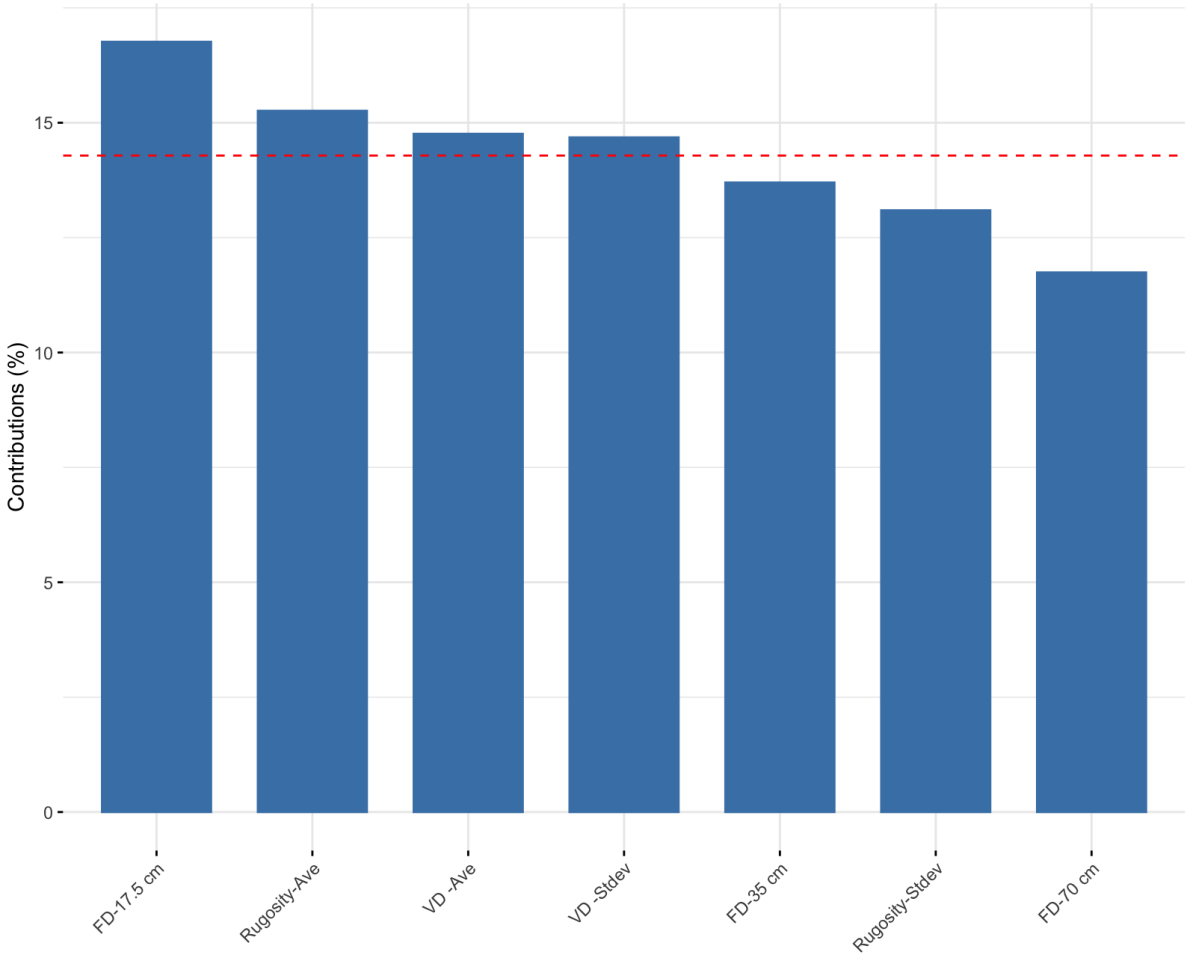

Figure 3.6a : Displaying the value contributions (%) of each variable for PC1. The dotted line representing the average contrbution of variables.

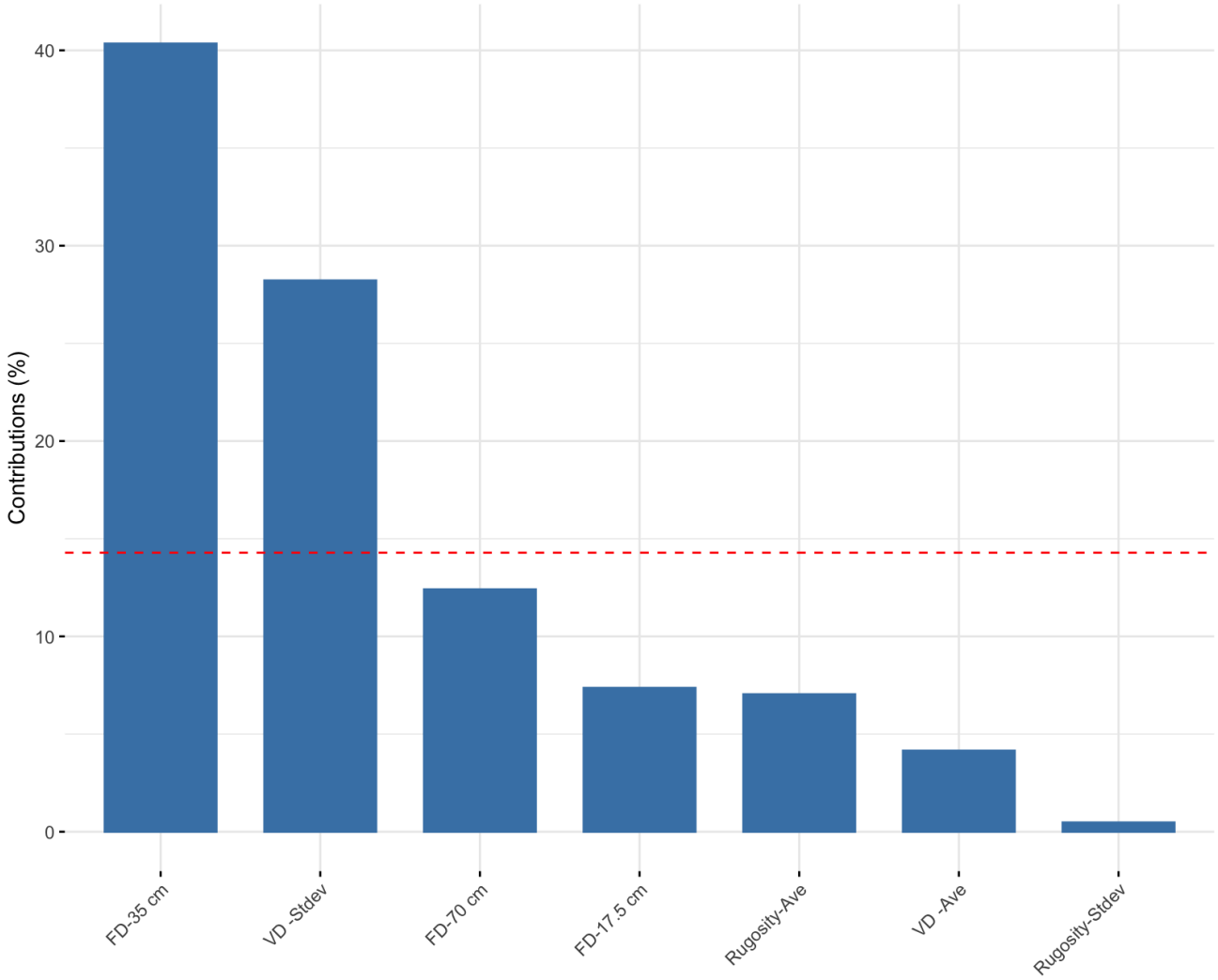

Figure 3.6b: Displaying the value contributions (%) of each variable for PC4. The dotted line representing the average contrbution of variables.

3.5 Canonical Correlation Analysis

The first canonical variates of BM and CM show a strong positive linear correlation of 0.796 (Figure 3.7). This means that changes in the BM dataset are strongly associated with changes in the CM dataset, according to the new variables (canonical variates) created for the analysis. The second pairs correlation is moderately high at 0.651, and suggests a relatively strong relationship, with changes in one variable often associated with changes in the other. While the third pair of canonical variates exhibits a more moderate correlation of 0.386, and suggests that changes in one of these variables are associated with changes in the other, but not as consistently as with a higher correlation. The coefficients used to build the two first pairs of

canonical variates were examined to determine which variables in the datasets contributing most to these relationships, given that the two first pairs have a much higher value than the rest.

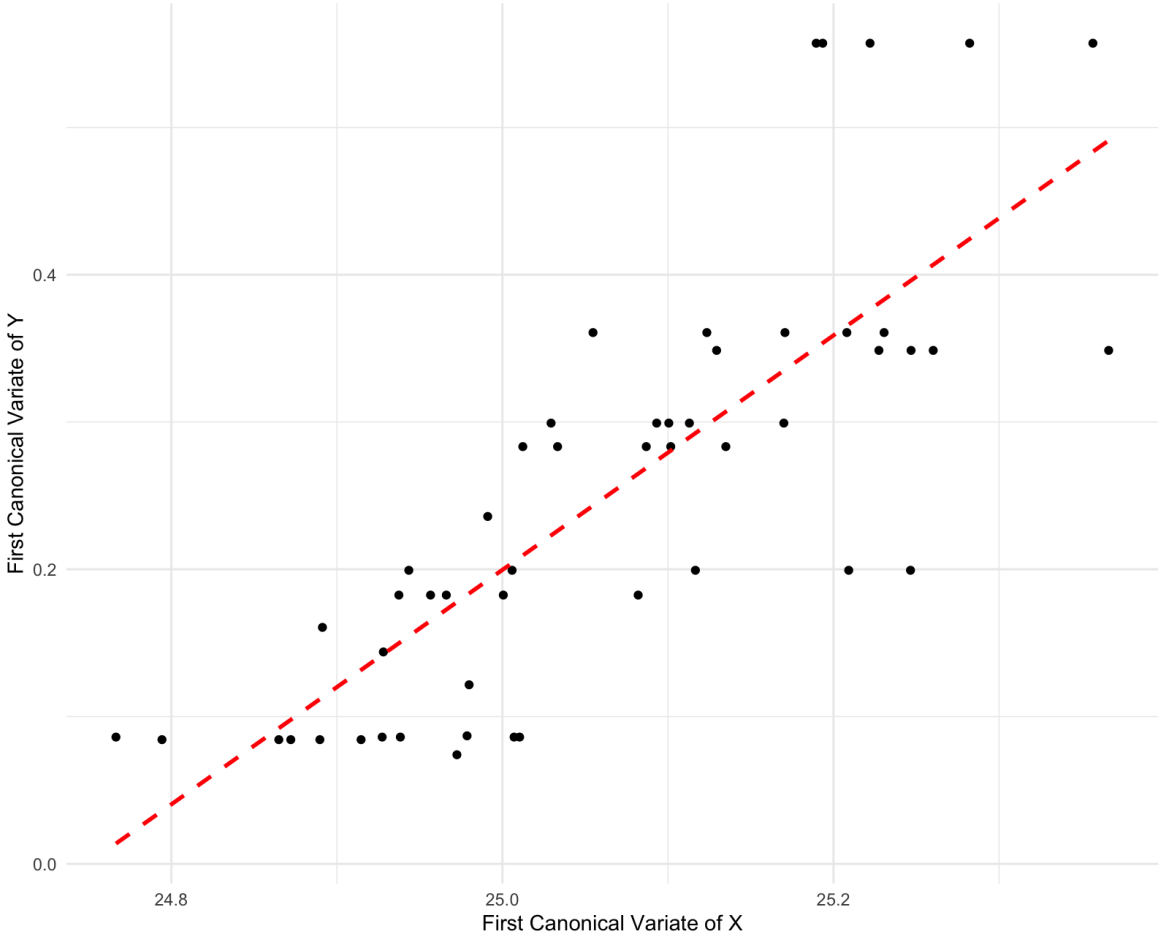

Figure 3.7: Scatterplot of First Canonical Variates with regression line indicating a strong linear relationship.

Table 5 : Displaying the coefficients of the canonical pairs. The sign of the coefficient indicates positive or negative relationship, while the magnitude of the coefficient indicates the strength of the relationship. The first pairs are most relevant, and their values are highlighted.

	Pair 1	Pair 2	Pair 3	Pair 4	Pair 5	Pair 6	Pair 7
Vector Dispersion	-2.46	-0.36	-1.58	0.28	3.91	3.19	2.93
Vector Dispersion SD	9.74	-7.60	1.46	-1.07	1.71	1.17	-8.61
Rugosity	-1.59	3.37	-4.28	-0.13	1.93	10.24	-1.20
Rugosity SD	-3.58	2.74	-11.84	-1.98	-5.73	14.69	4.89
FD 70 cm	8.59	4.15	10.26	-37.05	17.45	-20.48	14.25

FD 35 cm	6.71	7.14	12.55	8.07	-1.80	3.70	10.21
FD 17.5 cm	-2.08	7.25	-10.95	9.22	-5.45	-1.04	-13.27

Looking at the coefficients for the first pair based on CM (Table 5) , “Vector Dispersion SD” (9.74) and "FD 70 cm" (8.59) have the highest coefficients, suggesting that they have the strongest influence on the first canonical variate. In the second pair, “Vector Dispersion SD” shows a high negative coefficient (-7.60) indicating a negative relationship, while FD 35 cm (7.14) and FD 17.5 (7.25) indicating a positive relationship. Lastly, the Permutation test on the CCA results (with 10000 permutations) showed a *p*-value of 0.09249 which means that the result is not statistically significant at the 0.05 level.

3.6 Accuracy measurement

Using the meter as a reference point, the length from each edge of the quadrant that was placed on the mussel beds was measured as 44 cm wide. Actual length (AL) is the length measured by the meter. The error between AL and Measured length (ML) was 0.07 %.

Figure 3.8: Measuring length of the 3D model using Meshlab to test the accuracy of the model.

4 Discussion

The objective of this thesis was to construct a systematic procedure capable of generating quantitative data on blue mussel dynamics, utilizing the information extracted from 3D models of the mussels created via the SfM technique. In pursuit of this goal, the study endeavoured to find a correlation between fieldwork-collected biological datasets and the CM obtained from the 3D models generated through SfM. While some degree of correlation was observed between surface complexity and blue mussel biomass, this correlation failed to reach a level of statistical significance. Regardless, the established correlation does suggest the potential of this method, indicating that its further improvement could give valuable results. The study proposes that the fractal dimension might serve as the most effective complexity metric in illustrating the relationship between the surface complexity of the 3D models and the biological metrics. It should, however, be supplemented with additional complexity metrics to ensure a more holistic understanding of surface complexity. The outcomes of this study could have been impacted by several factors, including the limited biological sample size, the homogeneity of the mussels populations at the study sites, and variations in camera settings and distances during the process of image capture. To minimize the potential influence of these factors, it is recommended to increase the sample size, maintain a consistent scale and camera settings, and ensure accurate measurements. Once an optimized workflow is established, incorporating machine learning algorithms for object detection could significantly enhance workflow efficiency.

4.1 Exploring the correlation between CM and BM

Due to non-normally distributed data, the Spearman rank correlation was used (Schober et al., 2018) and this showed a poor correlation between the two groups, CM and BM, but a substantial relationship within the groups individually. This indicated a weak linear relationship between CM and BM, and a PCA of each of the groups was conducted in order to reduce the dimensions of the data. This would highlight the most important variables driving the variation in the dataset, and is often used to find a correlation between ecological metrics (Toosi et al., 2022). Neither the PCA of the CM nor the BM showed any clear grouping, meaning there was not much variability between the metrics. However since they are highly

correlated between each other separately, it suggested that using PCs could still be useful. A PCR is an effective technique for dealing with highly correlated predictor variables (Pires et al., 2008) and was performed with a number of PCs derived from CM as predictor variables. Cross-validation was used to establish the ideal number of PCs for the final PCR, and has proven to be effective for selecting the number of components (Josse & Husson, 2012). The rise in RMSEP from one to three components (Table 3), indicated that PC2 and PC3 might not have much information to add to the prediction.

The highest R-squared from the linear regression suggested that PC1-PC5 based on the CM could explain more than half of the variance in biomass (Table 4). The R-squared changes drastically for biomass and weight per mussel when adding PC4 , indicating that PC4 explain a substantial part of the variance for the variables. The plot with PC1 presented mostly a negative correlation, in particular with biomass and weight per mussel which corresponds with values from Table 3. The linear regression plot for PC2 shows a weak correlation with most of the BM, confirming the fact that PC2 has little information to provide to the prediction. The linear regression plot for PC4 shows a stronger positive correlation with the BM, validating the information given by Table 3 and 4.

The relationship between CM and BM was further investigated by performing a canonical correlation analysis to find more intricate or subtle relationships between the two datasets, given the fact that CCA can capture multivariate correlations that are not detectable by univariate correlation measures or by PCA, which only considers one dataset at a time (Palmer, 1993). The first pair of canonical variates showed a reasonably strong positive relationship, indicating that the datasets may be meaningfully related while the second pair showed a relationship that was moderately strong. The variables that contribute the most to these pairs were identified by looking at the coefficients of the first two pairs. The fractal dimension has been extensively utilized as a metric to quantify surface complexity (Bradbury & Reichelt, 1983). Coherent with the PCA results, fractal dimension had the strongest influence on the first and second canonical variates (Table 5), reinforcing the idea that fractal dimension could be the most useful complexity metric to extract using this method. However, "Vector Dispersion SD" also had a high coefficient for the first canonical variate (Table 5), indicating that this metric may add value as well. Lastly, the Permutation test on the CCA results (with 10000 permutations) showed a p-value of 0.09249 which means that the result is not statistically significant at the 0.05 level. In other words, there was no strong evidence to conclude that there

is a significant correlation between the two sets of variables based on this test. Nonetheless, based on the outcomes presented, SfM demonstrates its potential as a suitable technique for generating 3D models with information that can be utilized to acquire quantitative data on blue mussel size and biomass.

4.2 Observations and possible factors affecting the 3D models

There are several factors in this workflow to be taken into consideration. Firstly, the small biological sample collected have a limited statistical power and may not be able to detect significant differences or correlations, even if they exist in the population. Ideally, all of the collected quadrants would be used, but some of them had a low coverage of mussels, making their inclusion complicated and of little value. The homogeneity of the patches mussels photographed and collected during fieldwork made it more challenging to detect significant correlations with the CM. Nonetheless, identifying and sampling mussel patches with high variability proved to be a challenge, given the population dynamics in Hardangerfjorden and the established low variability of these populations (Strohmeier et al., 2022). Furthermore, when collecting and counting mussels, many of the smallest mussels might not have been collected due to their size making them challenging to collect, which could have influenced the size distribution within the samples.

The photos taken to create the 3D models could also have affected the results. Due to unfavourable weather conditions, drone image capturing was not carried out during the final study. However, as described in material & method, a test during good weather with a DJI Air 2s drone at various locations near Austevoll demonstrated high-quality imagery. Drones offer the advantage of accessing areas that are difficult or impossible to reach through other methods, but it is essential to consider their limitations, such as susceptibility to weather-related disruptions. In this thesis, photos were taken with both an Olympus TG-6 and a Samsung SM-G78, but due to the Olympus malfunctioning during sampling, only photos from the Samsung SM-G78 were used. Consequently, the photos were taken with different metering mode and exposure times to acquire the best quality, which could have affected the final 3D models. Yet, Meshroom, the 3D reconstruction software used, includes a camera calibration step in its pipeline. It uses information embedded in the images' metadata (EXIF data), such as the camera model, focal length, and sensor size, to estimate the camera's intrinsic parameters (Meshroom,

2021a). Nonetheless, Meshrooms automatic calibration may not perfectly account for all variations, especially if your images have a wide range of different exposure times.

The scale at which the images are taken (e.g., distance between the camera and the subject and camera sensor resolution) can also influence the level of detail captured and the overall accuracy of the 3D model. Meshroom detects key points (features) in each image and then matches them across multiple images (Westoby et al., 2012). The software is designed to handle variations in scale, rotation, and illumination by using scale-invariant feature detectors and descriptors, such as SIFT (Scale-Invariant Feature Transform) or AKAZE (Meshroom, 2021b). These methods are robust to changes in scale, which helps ensure that features can be matched even when images are taken from different distances. However, smaller scales (i.e., capturing images from a greater distance) generally result in lower resolution models, while larger scales (i.e., capturing images from a closer distance) can provide higher resolution and more accurate models. Closer distance will therefore have a smaller ground sampling distance (Westoby et al., 2012).

An article by Li & Lan (2019), discusses how reconstructions of objects (or scenes) using SfM based on monocular camera or multiple uncalibrated cameras are only possible up to an unknown scale. To recover the absolute scale, additional information or constraints are often needed. These can include known measurements of the object or scene, the use of calibrated cameras with known focal lengths, or the inclusion of external sensors (e.g., GPS, accelerometers) to provide information about the camera's position and orientation during the image acquisition process. This approach could have a potential to obtain absolute scale. However, an accuracy test was conducted and gave an error between the actual length and measured length to be only 0.07 %. Nevertheless, to minimize these potential issues, it would be recommended to maintain an even more consistent distance from the quadrants containing mussels when capturing images and to use calibrated cameras with similar exposure time to increase the accuracy of the models created by SfM.

4.3 Investigating the use of complexity metrics

Three different CM were calculated to describe surface complexity using the method described by Young et al., (2017). Rugosity has commonly been used to measure habitat complexity. Rugosity is easy to measure and calculate, making it a popular choice among researchers. In

the workflow suggested by Young et al., (2017), only a few chains were positioned over the topography. To capture more of the complexity, several chains were added (Figure 2.6). However, since rugosity is inherently tied to the surface area, it may not capture other aspects of habitat complexity, such as the spatial arrangement or distribution of features within a given area. This limitation could make rugosity less effective for assessing complexity on a microscale, where the arrangement and distribution of features might be more critical than the surface area itself (Loke & Chisholm, 2022). There was an indication that this might have been reflected in the results, with rugosity having the lowest correlation with BM and low contribution to the PCs (except PC1) and one of the canonical pairs.

Fractal dimension is another commonly metric used to calculate complexity, and can capture aspects of habitat structure that are not captured by rugosity, such as the degree of branching or clustering (Loke & Chisholm, 2022). Fractal dimension was the complexity metric that correlated the most to the BM, and with significant contribution to PC1 (FD 17.5cm) and PC4 (FD 35 cm) as well as having a strong influence on the two first pairs canonical variates (Table 5). The self-similarity and scale-invariant properties of fractal dimension might reveal important aspects of habitat structure that might capture the complexity on a microscale, making it a suitable measurement. Other research has suggested that fractal dimension may be correlated with certain biological variables, however, the strength of this correlation varies, and the results are not always consistent across different studies and contexts (Loke & Chisholm, 2022).

Vector dispersion is a less common complexity metric considered to be appropriate for measuring surface complexity in terms of surface angle variation. Due to its simple range (0-1) and positive response to increasing surface irregularity and sensitivity to biological or ecological population variables it can be a useful measurement (Carleton & Sammarco, 1987) In terms of this study, vector dispersion was not the most important contributor to describe the variance correlated to the BM. However, vector dispersion did have a large contribution to PC1 (Figure 3.6a) and Vector dispersion SD having the same for PCA 2 (Figure 3.6b), displaying its potential to describe complexity. Other similar studies have used vector dispersion to measure complexity at microscale. Carleton & Sammarco (1987) discovered that at fine scales (millimeter to centimeter), vector dispersion accounted for 36% of the variation in coral genus richness. However, Mccormick (1994) found that at coarser scales (meter), vector dispersion explained only 19%, 8%, and 2% of the variation in fish species richness on coral reefs,

respectively. In a more recent study conducted at the same location and similar scales, Torres-Pulliza et al., (2020) reported that surface height range accounted for a mere 4% of the variation in coral species richness. Nonetheless, it is worth noting that these results could be influenced by the different species under study, and this factor should be considered when interpreting the findings.

4.4 Recommendations for future research

In future studies applying the method used in this thesis, several improvements could enhance the outcomes. Firstly, increasing the sample size should help capture more variability within the biological datasets, although population dynamics may sometimes limit such variability. Secondly, ensuring consistent scale and camera settings during image collection could prove beneficial. While some research suggests that uncalibrated photos can produce accurate and precise models at small scales (Young et al., 2017), calibrated images could improve the results of SfM applications. Using advanced data processing techniques to account for differences in camera settings could also improve the results.

The scale at which images are captured significantly impacts the level of detail and overall accuracy of the 3D models generated using SfM. While current software can handle some variations in scale, future advancements in these methods might further improve the models. Li & Lan (2019) suggests a technique for recovering absolute scale in SfM based on motion constraints defined by a relative free fall motion between the camera and the object. The suggested closed-form analytical solution appears to function effectively in practice, but it also highlights the need to minimize uncertainties related to camera properties and experiment designs. To address potential issues with resolution and scale, it is recommended to maintain a consistent distance from the quadrants containing mussels during image capture and to use calibrated cameras with known exposure time. These steps can help enhance the accuracy of the models created using SfM.

This study suggests that the fractal dimension could potentially serve as the most powerful metric for depicting the correlation between surface complexity and biological variables. Utilizing this measurement at an extremely high resolution could effectively capture microscale details, though it may necessitate robust computational resources. Nevertheless, to

gain a comprehensive and in-depth understanding of surface complexity, this metric should be used in tandem with other CM. These could include metrics like vector dispersion or rugosity, among others, which may also be advantageous in providing a detailed representation of surface complexity. Slope is another potential metric that could be utilized, and it has already frequently used metric in marine studies (Friedman et al., 2012). Slope captures the steepness or incline of the surface of a model. It can provide information about the local shape and changes in the surface of the model. The complexity of a model can be inferred from the variety and intensity of its slopes (Friedman et al., 2012) .

Future research that combines the current approach with the capabilities of machine learning algorithms for object detection has the potential to greatly enhance this method. By employing object detection techniques, such as those trained using programs like U-Net, the workflow can be streamlined through the automatic recognition of mussel patches. Integrating this automation into the existing workflow could improve the efficiency of the image analysis process and such a workflow is visually presented in Figure 1.2. Preliminary results suggest that the algorithms used can successfully identify mussels, and with further annotation efforts, their performance can be further improved. By developing a workflow that combines the SfM technique, drones capable of surveying large areas, and machine learning algorithms to improve efficiency, there is a tremendous opportunity to enhance our understanding of blue mussels dynamics. This integrated approach enables the effective collection of quantitative data on blue mussel size, biomass, and coverage, leading to valuable insights into their population dynamics.

5 Conclusion

In conclusion, this thesis aimed to develop a systematic process for generating quantitative data on blue mussel dynamics by extracting information from 3D models created using the SfM technique. The study attempted to establish a correlation between fieldwork-collected datasets and CM derived from these 3D models. Although the results showed some correlation between the CM and BM, the relationship was not statistically significant. However, the correlation proves the potential of this method and that further developing this method could be valuable. The study suggests that fractal dimension could be the most useful complexity metric to describe the relationship between surface complexity of the 3D models and BM, but this metric should be used in conjunction with other CM to provide a more comprehensive understanding of surface complexity.

Factors such as limited biological sample size, homogeneity of mussels, and variations in camera settings and distances during image capture may have influenced the results. Minimizing possible errors inflicted by these factors would be beneficial. This would include increasing the sample size, ensuring consistent scale and camera settings. When a satisfying workflow is created, integrating machine learning algorithms for object detection would improve the workflow efficiency. This study, while not definitive, illustrates the potential of SfM as a viable technique for constructing 3D models. These models can subsequently serve as a foundation for generating comprehensive quantitative data. Such data can offer valuable insights into the dynamics of blue mussels, such as mussel size, total biomass, and coverage area, all of which correlate with the significant ecosystem services provided by these organisms. Gathering information beyond simply mapping blue mussel presence, can substantially enhance our understanding of their population dynamics, enabling both effective conservation measurements and sustainable utilization of these vital marine resources.

Bibliography

Agisoft. (2022). *Agisoft Metashape Professional* (Version 1.8.3). https://www.agisoft.com/

AliceVision. (2018). *Meshroom: A 3D reconstruction software*. https://github.com/alicevision/meshroom

Andersen, S. (2014). 'Køkkenmøddinger' (Shell Middens) in Denmark: A Survey. *Proceedings of the Prehistoric Society*, *66*, 361–384. https://doi.org/10.1017/S0079497X00001857

Andersen, S., Mortensen, Stein, & Strohmeier, Tore. (2016). *Meldinger om blåskjell som er forsvunnet – oppsummering for 2016 (Rapport fra Havforskningen nr. 4-2017)*. IMR. https://www.hi.no/hi/nettrapporter/rapport-fra-havforskningen/2017/hi-rapp_4-2017_blaskjell_sa

Anonymous. (1886). Poisonous Mussels from Impure Waters. *Science*, *ns-7*(159s), 175–176. https://doi.org/10.1126/science.ns-7.159S.175

Baden, S., Hernroth, B., & Lindahl, O. (2021). Declining Populations of Mytilus spp. In North Atlantic Coastal Waters—A Swedish Perspective. *Journal of Shellfish Research*, *40*(2), 269–296. https://doi.org/10.2983/035.040.0207

Baxter, T. I., Coombes, M. A., & Viles, H. A. (2022). The bioprotective properties of the blue mussel (Mytilus edulis) on intertidal rocky shore platforms. *Marine Geology*, *445*, 106734. https://doi.org/10.1016/j.margeo.2022.106734

Berge, J., Johnsen, G., Nilsen, F., Gulliksen, B., & Slagstad, D. (2005). Ocean temperature oscillations enable reappearance of blue mussels Mytilus edulis in Svalbard after 1000 year absence. *Marine Ecology-Progress Series - MAR ECOL-PROGR SER*, *303*, 167–175. https://doi.org/10.3354/meps303167

Beyer, J., Green, N. W., Brooks, S., Allan, I. J., Ruus, A., Gomes, T., Bråte, I. L. N., & Schøyen, M. (2017). Blue mussels (Mytilus edulis spp.) as sentinel organisms in coastal pollution monitoring: A review. *Marine Environmental Research*, *130*, 338–365. https://doi.org/10.1016/j.marenvres.2017.07.024

Bradbury, R., & Reichelt, R. (1983). Fractal Dimension of a Coral Reef at Ecological Scales. *Marine Ecology Progress Series*, *10*, 169–171. https://doi.org/10.3354/meps010169

Brooks, S. J., & Farmen, E. (2013). The Distribution of the Mussel Mytilus Species Along the Norwegian Coast. *Journal of Shellfish Research*, *32*(2), 265–270. https://doi.org/10.2983/035.032.0203

Carleton, J. H., & Sammarco, P. W. (1987). Effects of Substratum Irregularity on Success of Coral Settlement: Quantification by Comparative Geomorphological Techniques. *Bulletin of Marine Science*, *40*(1), 85–98.

Casella, E., Collin, A., Harris, D., Ferse, S., Bejarano, S., Parravicini, V., Hench, J. L., & Rovere, A. (2017). Mapping coral reefs using consumer-grade drones and structure from motion photogrammetry techniques. *Coral Reefs*, *36*(1), 269–275. https://doi.org/10.1007/s00338-016-1522-0

Chislock, M. F., Doster, Enrique, Zitomer, Rachel, & Wilson, A.E. (2013). Eutrophication: Causes, Consequences, and Controls in Aquatic Ecosystems. *Nature Education Knowledge*, *4*. https://www.nature.com/scitable/knowledge/library/eutrophication-causes-consequences-and-controls-in-aquatic-102364466/

Demmer, J., Robins, P., Malham, S., Lewis, M., Owen, A., Jones, T., & Neill, S. (2022). The role of wind in controlling the connectivity of blue mussels (Mytilus edulis L.) populations. *Movement Ecology*, *10*(1), 3. https://doi.org/10.1186/s40462-022-00301-0

Deur, D. E., & Turner, N. J. (2006). *Keeping It Living: Traditions of Plant Use and Cultivation on the Northwest Coast of North America*. University of Washington Press. http://ebookcentral.proquest.com/lib/bergen-ebooks/detail.action?docID=3444426

FAO. (2022). *The State of World Fisheries and Aquaculture 2022*. https://doi.org/10.4060/cc0461en

Filgueira, R., Strohmeier, T., & Strand, Ø. (2019). Regulating Services of Bivalve Molluscs in the Context of the Carbon Cycle and Implications for Ecosystem Valuation. In A. C. Smaal, J. G. Ferreira, J. Grant, J. K. Petersen, & Ø. Strand (Eds.), *Goods and Services of Marine Bivalves* (pp. 231–251). Springer International Publishing. https://doi.org/10.1007/978-3-319-96776-9_12

Fiskeridirektoratet. (2021). *Økt salg av oppdrettsfisk i 2021*. Fiskeridirektoratet. https://www.fiskeridir.no/Akvakultur/Nyheter/2022/okt-salg-av-oppdrettsfisk-i-2021

Friedman, A., Pizarro, O., Williams, S. B., & Johnson-Roberson, M. (2012). Multi-Scale Measures of Rugosity, Slope and Aspect from Benthic Stereo Image Reconstructions. *PLOS ONE*, *7*(12), e50440. https://doi.org/10.1371/journal.pone.0050440

Goldberg, E. D. (1975). The mussel watch—A first step in global marine monitoring. *Marine Pollution Bulletin*, *6*(7), 111. https://doi.org/10.1016/0025-326X(75)90271-4

Griwodz, C., Gasparini, S., Calvet, L., Gurdjos, P., Castan, F., Maujean, B., De Lillo, G., & Lanthony, Y. (2021). AliceVision Meshroom: An open-source 3D reconstruction

pipeline. *Proceedings of the 12th ACM Multimedia Systems Conference*, 241–247. https://doi.org/10.1145/3458305.3478443

Gundersen, H., Bryan, T., Chen, W., Moy, F., Sandman, A., Sundblad, G., Schneider, S., Andersen, J., Langaas, S., & Walday, M. (2017). *Ecosystem Services In the Coastal Zone of the Nordic Countries*. https://doi.org/10.6027/TN2016-552

HELCOM. (2018). *State of the Baltic Sea – Second HELCOM holistic assessment 2011-2016*. https://www.helcom.fi/baltic-sea-trends/holistic-assessments/state-of-the-baltic-sea-2018/reports-and-materials/

Icalc, Inc. (2020). *SketchAndCalc Area Calculator* (5.1.2). https://www.sketchandcalc.com/

Jaboyedoff, M., Oppikofer, T., Abellán, A., Derron, M.-H., Loye, A., Metzger, R., & Pedrazzini, A. (2012). Use of LIDAR in landslide investigations: A review. *Natural Hazards*, *61*(1), 5–28. https://doi.org/10.1007/s11069-010-9634-2

Jones, S. J., Lima, F. P., & Wethey, D. S. (2010). Rising environmental temperatures and biogeography: Poleward range contraction of the blue mussel, Mytilus edulis L., in the western Atlantic. *Journal of Biogeography*, *37*(12), 2243–2259. https://doi.org/10.1111/j.1365-2699.2010.02386.x

Josse, J., & Husson, F. (2012). Selecting the number of components in PCA using cross-validation approximations. *Computational Statistics & Data Analysis*, *56*. https://doi.org/10.1016/j.csda.2011.11.012

Kotta, J., Futter, M., Kaasik, A., Liversage, K., Rätsep, M., Barboza, F. R., Bergström, L., Bergström, P., Bobsien, I., Díaz, E., Herkül, K., Jonsson, P. R., Korpinen, S., Kraufvelin, P., Krost, P., Lindahl, O., Lindegarth, M., Lyngsgaard, M. M., Mühl, M., … Virtanen, E. (2020). Cleaning up seas using blue growth initiatives: Mussel farming for eutrophication control in the Baltic Sea. *Science of The Total Environment*, *709*, 136144. https://doi.org/10.1016/j.scitotenv.2019.136144

Leiserson, C. E., Thompson, N. C., Emer, J. S., Kuszmaul, B. C., Lampson, B. W., Sanchez, D., & Schardl, T. B. (2020). There's plenty of room at the Top: What will drive computer performance after Moore's law? *Science*, *368*(6495), eaam9744. https://doi.org/10.1126/science.aam9744

Li, L., & Lan, H. (2019). Recovering absolute scale for Structure from Motion using the law of free fall. *Optics & Laser Technology*, *112*, 514–523. https://doi.org/10.1016/j.optlastec.2018.11.045

Lin, S., & Lin, F. (2006). Towards an Ecological Perspective on the Evolution of Online Communities of Practice. *Towards an Ecological Perspective on the Evolution of Online Communities of Practice*, *6*, 134a–134a. https://doi.org/10.1109/HICSS.2006.493

Loeb, S., L., & Spacie, A. (1994). *Biological Monitoring of Aquatic Systems*. CRC Press.

Loke, L. H. L., & Chisholm, R. A. (2022). Measuring habitat complexity and spatial heterogeneity in ecology. *Ecology Letters*, *25*(10), 2269–2288. https://doi.org/10.1111/ele.14084

Lovshin, L. L. (1996). Aquaculture: Biology and ecology of cultured species: Gilbert Barnabe (Editor), Ellis Horwood, London, 1994, 403 pp., Hardback, £24.00, ISBN 0-13-482324-9. *Aquaculture*, *140*(4), 383–384. https://doi.org/10.1016/S0044-8486(96)90026-5

Mafra, L. L., Bricelj, V. M., Ouellette, C., & Bates, S. S. (2010). Feeding mechanics as the basis for differential uptake of the neurotoxin domoic acid by oysters, Crassostrea virginica, and mussels, Mytilus edulis. *Aquatic Toxicology*, *97*(2), 160–171. https://doi.org/10.1016/j.aquatox.2010.01.009

Malone, T. C., & Newton, A. (2020). The Globalization of Cultural Eutrophication in the Coastal Ocean: Causes and Consequences. *Frontiers in Marine Science*, *7*. https://www.frontiersin.org/articles/10.3389/fmars.2020.00670

Mandelbrot, B. (1983). *The Fractal Geometry of nature* (3rd ed.). W. H. Freeman and Comp.

McCormick, M. (1994). Comparison of Field Methods for Measuring Surface-Topography and Their Associations with a Tropical Reef Fish Assemblage. *Marine Ecology Progress Series*, *112*(1–2), 87–96. https://doi.org/10.3354/meps112087

McNeel, R. (2010). *Rhinoceros 3D,* (Version 7.0.). Robert McNeel & Associates, Seattle, WA.

Meier, H. E. M., Höglund, A., Eilola, K., & Almroth-Rosell, E. (2017). Impact of accelerated future global mean sea level rise on hypoxia in the Baltic Sea. *Climate Dynamics*, *49*(1), 163–172. https://doi.org/10.1007/s00382-016-3333-y

Meshlab. (2022). *Mehslab* (2022.02). https://www.meshlab.net/

Meshroom. (2021a). *Capturing—Meshroom v2021.0.1 documentation*. https://meshroom-manual.readthedocs.io/en/latest/capturing/capturing.html

Meshroom. (2021b). *FeatureExtraction—Meshroom v2021.0.1 documentation*. FeatureExtraction. https://meshroom-manual.readthedocs.io/en/latest/feature-documentation/nodes/FeatureExtraction.html

Mortensen, S., Skår, C., & Bøgwald, M. (2021, May 12). *The surveillance and control programme for bonamiosis and marteiliosis in European flat oysters, Ostrea edulis, and blue mussels, Mytilus sp. In Norway in 2020*. Havforskningsinstituttet. https://www.hi.no/hi/nettrapporter/rapport-fra-havforskningen-en-2021-21

Newell, R., & Moran, D. (1989). *Species Profiles: Life Histories and Environmental Requirements of Coastal Fishes and Invertebrates (North and Mid-Atlantic)*.

https://www.semanticscholar.org/paper/Species-Profiles%3A-Life-Histories-and-Environmental-Newell-Moran/45a1ebf9cda38772ee9493a2c7252249c667a17c

Nøland, Helena. (2021). *Endring i forekomst av blåskjell (Mytilus edulis) i Oslofjorden. - Analyse av populasjoner over tid og mulige årsaker til variasjon.* University of Oslo.

Norling, P. (2009). *Importance of blue mussels for biodiversity and ecosystem functioning in subtidal habitats*. http://urn.kb.se/resolve?urn=urn:nbn:se:su:diva-27339

Palmer, M. W. (1993). Putting Things in Even Better Order: The Advantages of Canonical Correspondence Analysis. *Ecology*, *74*(8), 2215–2230. https://doi.org/10.2307/1939575

Pires, J. C. M., Martins, F. G., Sousa, S. I. V., Alvim-Ferraz, M. C. M., & Pereira, M. C. (2008). Selection and validation of parameters in multiple linear and principal component regressions. *Environmental Modelling & Software*, *23*(1), 50–55. https://doi.org/10.1016/j.envsoft.2007.04.012

Portosi, V., Laneve, D., Falconi, M. C., & Prudenzano, F. (2019). Advances on Photonic Crystal Fiber Sensors and Applications. *Sensors*, *19*(8), Article 8. https://doi.org/10.3390/s19081892

Poulsen, R., Gravert, T. K. O., Tartara, A., Bensen, H. K., Gunnarsen, K. C., Dicová, K., Nielsen, N. J., & Christensen, J. H. (2021). A case study of PAH contamination using blue mussels as a bioindicator in a small Greenlandic fishing harbor. *Marine Pollution Bulletin*, *171*, 112688. https://doi.org/10.1016/j.marpolbul.2021.112688

R Core Team. (2022). *R: A language and environment for statistical computing*. R Foundation for Statistical Computing, Vienna, Austria. https://www.R-project.org/.

Reid, G. K., Lefebvre, S., Filgueira, R., Robinson, S. M. C., Broch, O. J., Dumas, A., & Chopin, T. B. R. (2020). Performance measures and models for open-water integrated multi-trophic aquaculture. *Reviews in Aquaculture*, *12*(1), 47–75. https://doi.org/10.1111/raq.12304

Reig, B., Heacock, L., Geras, K. J., & Moy, L. (2020). Machine Learning in Breast MRI. *Journal of Magnetic Resonance Imaging : JMRI*, *52*(4), 998–1018. https://doi.org/10.1002/jmri.26852

Riisgård, H. U., Larsen, P. S., & Pleissner, D. (2014). Allometric equations for maximum filtration rate in blue mussels Mytilus edulis and importance of condition index. *Helgoland Marine Research*, *68*(1), Article 1. https://doi.org/10.1007/s10152-013-0377-9

Ruiz, G. M., Fofonoff, P. W., Steves, B., Foss, S. F., & Shiba, S. N. (2011). Marine invasion history and vector analysis of California: A hotspot for western North America:

Marine invasion history for western North America. *Diversity & Distributions*, *17*(2), 362–373. https://doi.org/10.1111/j.1472-4642.2011.00742.x

Schober, P., Boer, C., & Schwarte, L. A. (2018). Correlation Coefficients: Appropriate Use and Interpretation. *Anesthesia and Analgesia*, *126*(5), 1763–1768. https://doi.org/10.1213/ANE.0000000000002864

Sea, M. A., Hillman, J. R., & Thrush, S. F. (2022). The influence of mussel restoration on coastal carbon cycling. *Global Change Biology*, *28*(17), 5269–5282. https://doi.org/10.1111/gcb.16287

Seed, R. (1992). Systematics Evolution and Distribution of Mussels Belonging To the Genus Mytilus—An Overview. *American Malacological Bulletin*, *9*(2), 123–137.

Smaal, A. C., Ferreira, J. G., Grant, J., Petersen, J. K., & Strand, Ø. (Eds.). (2019). *Goods and Services of Marine Bivalves*. Springer International Publishing. https://doi.org/10.1007/978-3-319-96776-9

Snavely, N., Seitz, S., & Szeliski, R. (2007, December 11). *Modeling the World from Internet Photo Collections | SpringerLink*. https://doi.org/10.1007/s11263-007-0107-3

Sousa, J., & Gonçalves, G. (2011). Unmanned vehicles for environmental data collection. *Clean Technologies and Environmental Policy*, *13*, 369–380. https://doi.org/10.1007/s10098-010-0313-5

Strohmeier, Tore, Strand, Øivind, Gatti, Paul, & Aguera Garcia, Antonio. (2022, November 5). *Overvåking av blåskjellbestanden – grunnundersøkelse 2021 og 2022*. Havforskningsinstituttet. https://www.hi.no/hi/nettrapporter/rapport-fra-havforskningen-2022-38

Suchanek, T. (1992). Extreme biodiversity in the marine environment: Mussel bed communities of Mytilus californianus. *Northwest Environmental Journal*, *8*, 150–152.

Thompson, R. J. (1979). Fecundity and Reproductive Effort in the Blue Mussel (Mytilus edulis), the Sea Urchin (Strongylocentrotus droebachiensis), and the Snow Crab (Chionoecetes opilio) from Populations in Nova Scotia and Newfoundland. *Journal of the Fisheries Research Board of Canada*, *36*(8), 955–964. https://doi.org/10.1139/f79-133

Toosi, N. B., Soffianian, A. R., Fakheran, S., & Waser, L. T. (2022). Mapping disturbance in mangrove ecosystems: Incorporating landscape metrics and PCA-based spatial analysis. *Ecological Indicators*, *136*, 108718. https://doi.org/10.1016/j.ecolind.2022.108718

Torres-Pulliza, D., Dornelas, M. A., Pizarro, O., Bewley, M., Blowes, S. A., Boutros, N., Brambilla, V., Chase, T. J., Frank, G., Friedman, A., Hoogenboom, M. O., Williams, S., Zawada, K. J. A., & Madin, J. S. (2020). A geometric basis for surface habitat

complexity and biodiversity. *Nature Ecology & Evolution*, *4*(11), Article 11. https://doi.org/10.1038/s41559-020-1281-8

Torrissen,O, Nordberg,B, Viswanath, K, Strohmeier, T., Strand, Øivind, Naustvoll, Lars-Johan, & Svåsand, T. (2018). *Framtidsrettet matproduksjon i kyst og fjord – En vurdering av muligheter for økt sjømatproduksjon i Norge*. https://www.hi.no/hi/nettrapporter/rapport-fra-havforskningen/2018/23-2018_framtidsrettet_mat_1408

van der Merwe, D., Burchfield, D. R., Witt, T. D., Price, K. P., & Sharda, A. (2020). Chapter One—Drones in agriculture. In D. L. Sparks (Ed.), *Advances in Agronomy* (Vol. 162, pp. 1–30). Academic Press. https://doi.org/10.1016/bs.agron.2020.03.001

Ventura, D., Grosso, L., Pensa, D., Casoli, E., Mancini, G., Valente, T., Scardi, M., & Rakaj, A. (2023). Coastal benthic habitat mapping and monitoring by integrating aerial and water surface low-cost drones. *Frontiers in Marine Science*, *9*. https://doi.org/10.3389/fmars.2022.1096594

Westerbom, M., Kilpi, M., & Mustonen, O. (2002). Blue mussels, Mytilus edulis, at the edge of the range: Population structure, growth and biomass along a salinity gradient in the north-eastern Baltic Sea. *Marine Biology*, *140*(5), 991–999. https://doi.org/10.1007/s00227-001-0765-6

Westoby, M. J., Brasington, J., Glasser, N. F., Hambrey, M. J., & Reynolds, J. M. (2012). 'Structure-from-Motion' photogrammetry: A low-cost, effective tool for geoscience applications. *Geomorphology*, *179*, 300–314. https://doi.org/10.1016/j.geomorph.2012.08.021

Yanovski, R., Nelson, P. A., & Abelson, A. (2017). Structural Complexity in Coral Reefs: Examination of a Novel Evaluation Tool on Different Spatial Scales. *Frontiers in Ecology and Evolution*, *5*. https://doi.org/10.3389/fevo.2017.00027

Young, G. C., Dey, S., Rogers, A. D., & Exton, D. (2017). Cost and time-effective method for multi-scale measures of rugosity, fractal dimension, and vector dispersion from coral reef 3D models. *PLOS ONE*, *12*(4), e0175341. https://doi.org/10.1371/journal.pone.0175341

Young, Grace, G. C. (2018, May 12). *Rhino-Python-3D-Coral-Reefs/README.txt at master · gracecalvertyoung/Rhino-Python-3D-Coral-Reefs*. GitHub. https://github.com/gracecalvertyoung/Rhino-Python-3D-Coral-Reefs

Appendix A – Tables and figures

Table 6: Biological metrics with calculated biomass(g/m^2) and numbers (n/m^2)

Quadrant	Biomass(g)	g/m²	Number of Mussels (n)	n/m²	Mode	Mean	Median	Average Weight Per Mussel (g)
1	4910	30678	4576	28600	4	15.19	13	34.34
2	2450	15312	2368	14800	3	12.65	12	16.55
3	1230	12611	3321	34501	5	10.94	10	2.97
4	1050	14780	3008	42306	4	10.01	9	2.79
5	4000	25000	2008	12550	18	23.76	24	15.94
6	940	13662	1664	24186	3	9.73	6	9.04
10	2973	18581	8352	52200	3	9.87	6	11.39
13	1857	11606	2472	15450	4	8.89	7	6.01
15	496	9810	3008	59493	3	6.65	5	2.63
16	2629	16431	6240	39000	4	8.78	6	13.48
18	1593	9956	3360	21000	4	10.93	11	15.17
19	2892	18075	4448	27800	4	10.87	7	20.81
22	1166	9109	1584	12375	16	12.00	13	11.78
23	1149	9449	5664	46578	3	8.19	6	6.49
24	1156	7225	2688	16800	2	10.70	7.5	13.76

Table 7: Complexity metrics with vector dispersion (VD), vector dispersion standard deviation, rugosity, rugosity standard deviation, and the different fractal dimension (FD) (70 cm, 35 cm and 17.5 cm)

Quadrant	VD Average	VD SD	Rugosity Average	Rugosity SD	FD 70 cm	FD 35 cm	FD 17.5 cm
Q1*	0.0949	0.0518	0.9187	0.0335	2.0083	2.0268	2.0450
Q1_1	0.0671	0.0430	0.9247	0.0389	2.0029	2.0168	2.0128
Q1_2	0.0720	0.0678	0.9282	0.0424	1.9996	2.0134	2.0095
Q1_3	0.0494	0.0386	0.9450	0.0244	2.0080	2.0108	2.0087
Q1_4	0.0506	0.0438	0.9440	0.0374	2.0050	2.0102	2.0090
Q2*	0.1244	0.0342	0.9176	0.0357	2.0021	2.0112	2.0112
Q2_1	0.0667	0.0561	0.9377	0.0345	2.0026	2.0069	2.0116
Q2_2	0.0598	0.0494	0.9328	0.0361	2.0019	2.0082	2.0088
Q2_3	0.0396	0.0302	0.9298	0.0324	2.0032	2.0118	2.0127
Q2_4	0.0356	0.0231	0.9329	0.0274	2.0011	2.0043	2.0111
Q3	0.0567	0.0294	0.9053	0.0605	2.0046	2.0058	2.0116
Q4	0.0156	0.0081	0.9800	0.0105	2.0016	2.0006	2.0019
Q5*	0.1551	0.0476	0.9128	0.0317	2.0137	2.0353	2.0468
Q5_1	0.0536	0.0414	0.9717	0.0222	2.0055	2.0188	2.0116
Q5_2	0.0536	0.0384	0.9761	0.0155	2.0054	2.0139	2.0181

Q5_3	0.0299	0.0244	0.9795	0.0186	2.0091	2.0035	2.0098
Q5_4	0.0563	0.0347	0.9710	0.0147	2.0042	2.0131	2.0181
Q6	0.0474	0.0257	0.8866	0.0494	2.0016	2.0055	2.0195
Q10*	0.1645	0.0522	0.9071	0.0334	2.0048	2.0229	2.0373
Q10_1	0.0747	0.0386	0.9564	0.0194	2.0125	2.0104	2.0207
Q10_2	0.0524	0.0331	0.9569	0.0554	2.0090	2.0224	2.0168
Q10_3	0.0726	0.0467	0.9568	0.0265	2.0055	2.0052	2.0301
Q10_4	0.0450	0.0286	0.9786	0.0178	2.0059	2.0038	2.0139
Q13*	0.1195	0.0446	0.9372	0.0306	2.0109	2.0051	2.0094
Q13_1	0.0316	0.0213	0.9864	0.0057	2.0023	2.0030	2.0065
Q13_2	0.0463	0.0265	0.9774	0.0149	2.0009	2.0018	2.0117
Q13_3	0.0255	0.0155	0.9870	0.0075	2.0005	2.0032	2.0070
Q13_4	0.0435	0.0209	0.9784	0.0144	2.0036	2.0026	2.0072
Q15	0.0494	0.0244	0.9383	0.0290	2.0001	2.0048	2.0075
Q16*	0.2060	0.0616	0.8847	0.0436	2.0128	2.0191	2.0559
Q16_1	0.0800	0.0348	0.9565	0.0165	2.0068	2.0182	2.0358
Q16_2	0.0657	0.0331	0.9672	0.0189	2.0021	2.0077	2.0221
Q16_3	0.0883	0.0476	0.9371	0.0563	2.0129	2.0162	2.0355
Q16_4	0.0528	0.0260	0.9772	0.0080	2.0032	2.0082	2.0116
Q18*	0.2053	0.0363	0.8931	0.0243	1.9942	2.0121	2.0190
Q18_1	0.0603	0.0235	0.9714	0.0165	2.0040	2.0025	2.0113
Q18_2	0.0703	0.0262	0.9716	0.0125	2.0010	2.0020	2.0102
Q18_3	0.0645	0.0315	0.9714	0.0116	2.0009	2.0049	2.0144
Q18_4	0.0645	0.0299	0.9753	0.0121	2.0030	2.0049	2.0095
Q19*	0.2026	0.0593	0.8481	0.0653	2.0274	2.0420	2.0898
Q19_1	0.0695	0.0421	0.9424	0.0302	2.0046	2.0453	2.0207
Q19_2	0.0749	0.0326	0.9530	0.0243	2.0094	2.0184	2.0190
Q19_3	0.0768	0.0528	0.9357	0.0376	2.0092	2.0157	2.0359
Q19_4	0.0720	0.0398	0.9447	0.0413	2.0086	2.0328	2.0295
Q22	0.0483	0.0204	0.9318	0.0291	1.9997	2.0033	2.0099
Q23	0.0431	0.0222	0.9446	0.0224	2.0019	2.0028	2.0091
Q24*	0.0184	0.0109	0.9935	0.0026	2.0004	2.0019	2.0034
Q24_1	0.0032	0.0031	0.9986	0.0007	2.0002	2.0010	2.0007
Q24_2	0.0042	0.0035	0.9983	0.0009	2.0001	2.0001	2.0014
Q24_3	0.0040	0.0029	0.9934	0.0234	2.0001	2.0009	2.0011
Q24_4	0.0052	0.0050	0.9978	0.0014	2.0007	2.0012	2.0014

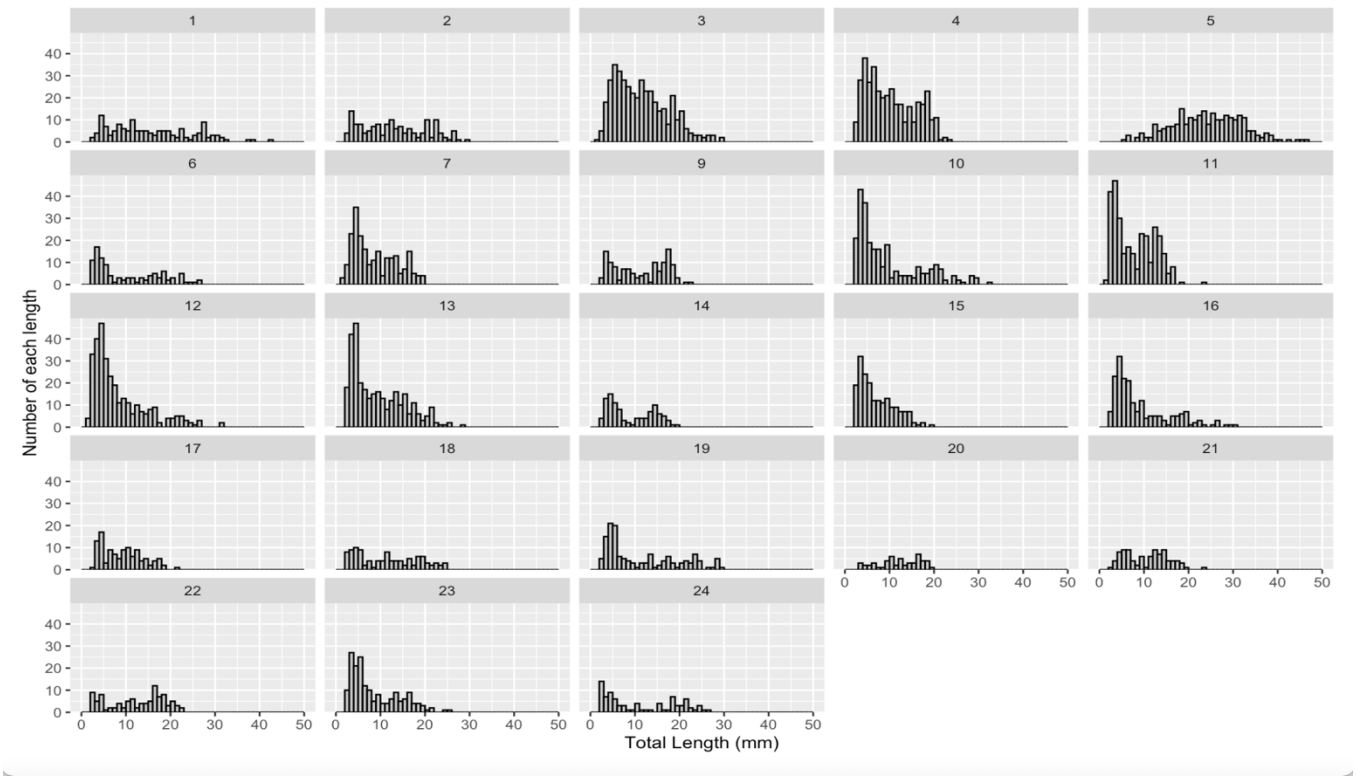

Figure 5.1: Length distribution for the mussels size of 23 quadrants with mussels.

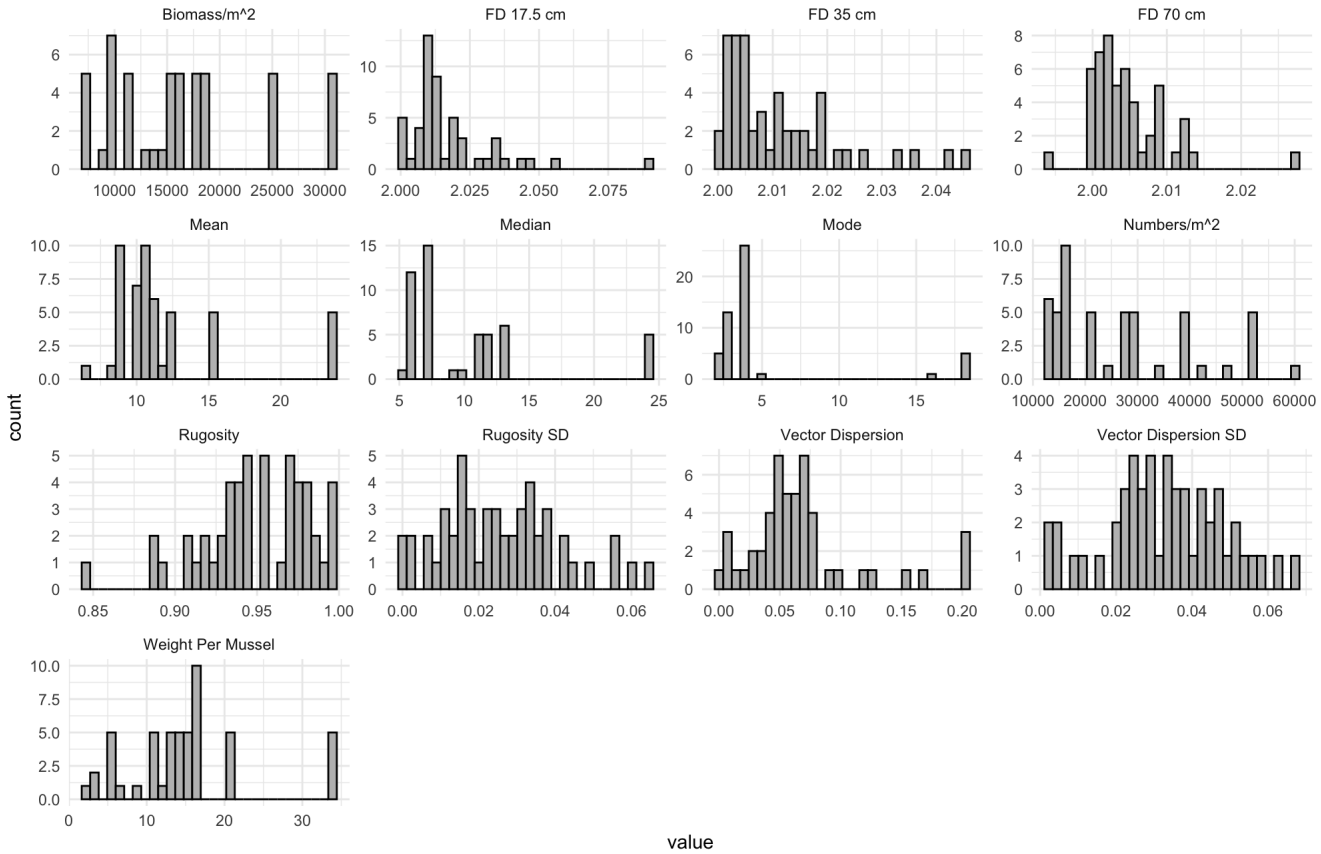

Figure 5.2. Histograms illustrating the distribution of complexity metrics and biological metrics .

Appendix B – Models

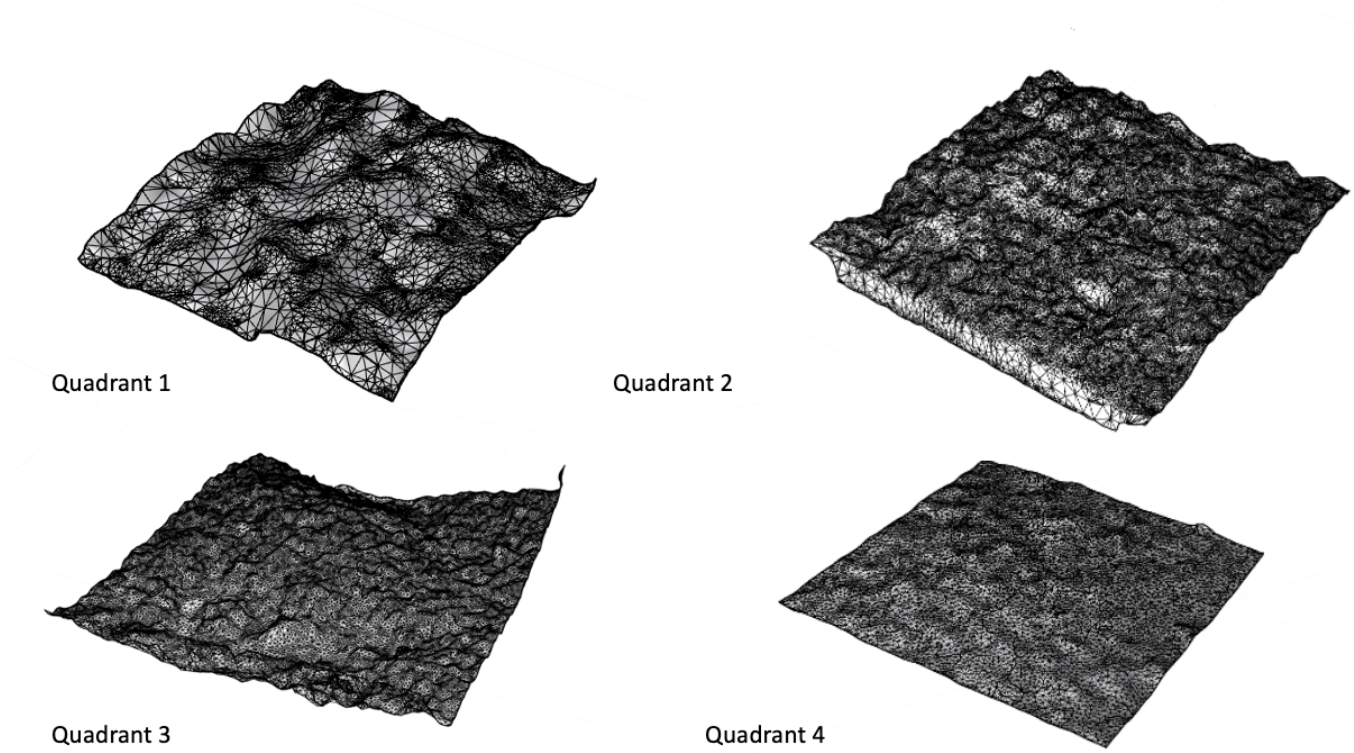

Figure 5.3: Models of quadrant 1 to 4.

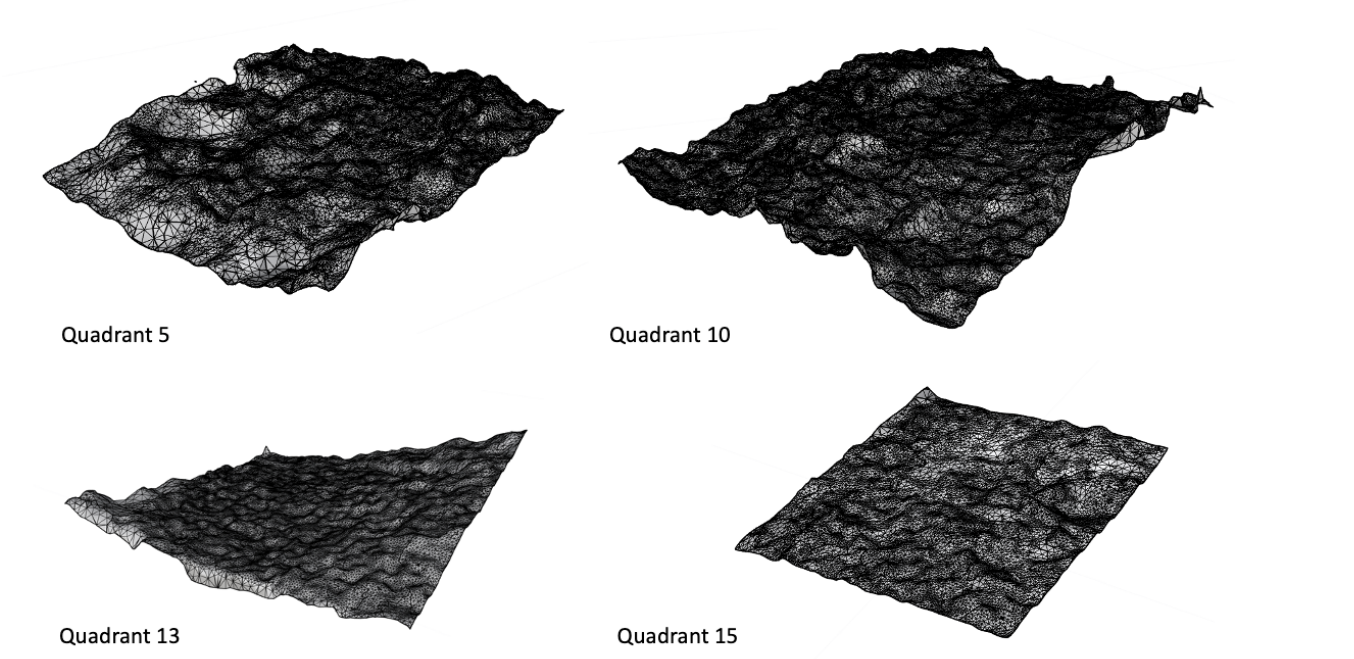

Figure 5.4: Models of quadrant 5, 10 , 13 and 15.

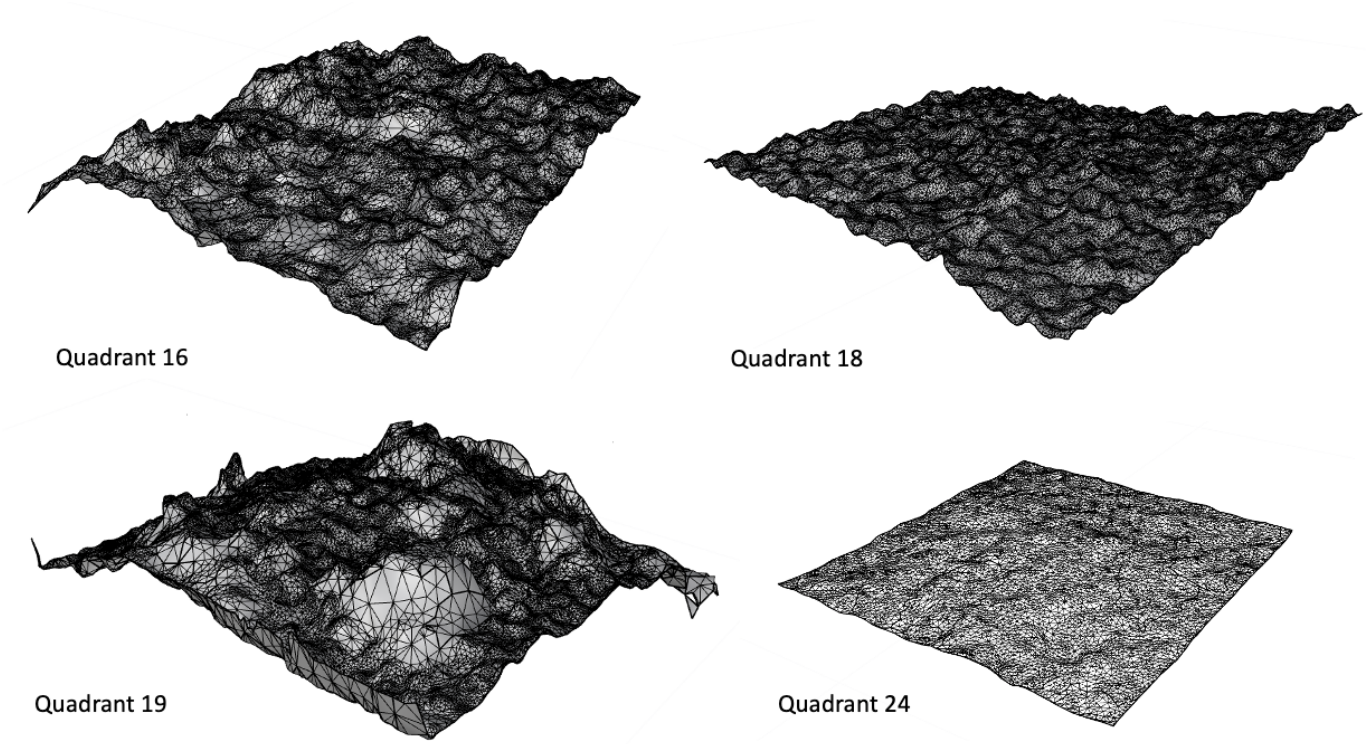

Figure 5.5: Models of quadrant 16, 18, 19 and 24.